Politecnico di Milano

Mechanics Department

Master of Science in Mechanical Engineering

Evaluation and Improvement of Digital Image Correlation Uncertainty in Dynamic Conditions

Supervisor: Prof. Emanuele ZAPPA

Master of Science Thesis by:
Ali MATINMANESH
Matr. N.767195

July 2013

Contents

Acknowledgement

First of all, I really appreciate my supervisor, Professor Emanuele Zappa for all the kindness and help, he provided me during the development of the thesis. Moreover, helps and advices of Dr. Paolo Mazzoleni during every step of this work were remarkably important.

I would also like to thank my father, my mother and my brother for all their supports. Finally, I thank my best friends Omid and Ramin for being like a brother to me, during all these years.

List of Figures

List of Tables

Abstract

Even though Digital Image Correlation (DIC) is a widely used optical full field measurement method, it still needs further performance investigations, when it comes to dynamic conditions. In dynamics, dealing with a moving target, causes a motion effect (i.e. blurring) on the acquired images. This factor is an important source of uncertainty that needs to be quantified. Therefore, the present study aims to evaluate and improve DIC's uncertainty in dynamic conditions. The study focuses on 2D DIC. In the case of 3D DIC similar problems will arise and therefore, a complete understanding of two dimensional conditions will be of great help to further studies which deal with 3D conditions. The whole work can be divided in to two main parts. In the first part, two different methods to simulate the motion effect on a reference image are proposed, discussed and validated. These methods allow simulating the acquired images in a real dynamic test and estimating the measurement uncertainty caused by the motion effect. The validation was performed by conducting several harmonic vibration tests. The results show good agreement between the experiments and the simulations, proving the proposed technique to be an effective method for motion induced uncertainty estimation. In the second part of the study a numerical technique was proposed to estimate the motion effect present in an acquired image. This technique gives two main advantages. First of all, since the motion effect itself has a known influence on the uncertainty of measurement (first part of the study), we will be able to predict the DIC's uncertainty by just having the acquired image and the static one. Furthermore, this numerical technique will be used to improve the uncertainty of DIC in dynamic applications. In this way the bias error and the uncertainty of the measurements will be considerably decreased.

Key words: Digital Image Correlation, Uncertainty, Deconvolution, Dynamics

CHAPTER 1

Introduction and Thesis Outline

Over the recent years, optical full field measurement methods have been widely used in experimental mechanics. The main techniques are photo elasticity, moiré, holographic and speckle interferometry, grid method and digital image correlation (DIC) [1]. Digital Image Correlation is a powerful technique, which has been mostly used in static applications. A group of articles have focused on quantification of performances of this method [1, 4-17]. They implemented a finite element procedure or presented a theoretical calculation technique to estimate the measurement uncertainty. These studies are all conducted in static conditions.

More recently, in some researches, DIC has been implemented also in dynamic applications such as mode shape recognition [23, 24, 26, 28] and vibration analysis [25, 27]. Although some of these studies have performed an uncertainty analysis of the measurement in that particular application [20-28], there seems to be an absolute need of further investigations of DIC performances, to analyze the measuring uncertainty in generic dynamic conditions. The performances of DIC technique, depends on a set of static and dynamic parameters; the former include: image resolution and blurring, lighting conditions and processing parameters. As for the dynamics, the motion parameters (mainly the instantaneous velocity) and the shutter time are usually considered relevant in image-base measurement uncertainty assessment [2, 3].

In dynamics, dealing with a moving target, causes a motion effect (i.e. blurring) on the acquired images. This motion effect would not exist, if the acquisition was instantaneous but in reality it is not a valid assumption to be made. The so called exposure time or the effective duration that a camera's shutter is open, is usually not negligible in respect to the velocity of the target. This means that the target slightly displaces during the exposure time which makes a single dot on the target to appear as a stripe on the acquired image.

This factor is an important source of uncertainty that needs to be quantified. Therefore, the present study aims to perform a systematic uncertainty assessment of DIC method in general dynamic applications. The study focuses on 2D DIC. In the case of 3D DIC similar problems will arise and therefore, a complete understanding of two dimensional conditions will be of great help to further studies which deal with 3D conditions.

The whole work can be divided in to two main parts. The first part, aims to analyze the effect of dynamics on the DIC uncertainty by proposing numerical and experimental approaches. The numerical approach is based on implementing two innovative methods to simulate the motion effect on a reference image. These numerical methods will allow us to keep all the other uncertainty sources under control and to explore the effect of dynamics. The performances of the two methods are then evaluated in different dynamic conditions. With these models and a given image of the target, it is possible to simulate the dynamic test and create a set of images that simulate the ones that would be obtained from a real test, with a known imposed vibration law. The simulated image set will be analyzed with the DIC technique and the discrepancy between the imposed and the estimated time histories will be utilized to estimate the uncertainty.

In the second part of the study a numerical technique is proposed to estimate the motion effect present in an acquired image. This technique gives two main advantages. First, since the motion effect itself has a known influence on the uncertainty of measurement (thanks to the first part of the study), we will be able to predict the DIC's uncertainty by just having an acquired image. Second, this numerical technique will be used to improve the uncertainty of DIC in dynamic applications.

The main body of this work is organized as below:

- **Chapter 2** discusses the state of the art regarding the DIC uncertainty assessment in the case of general dynamic applications.
- **Chapter 3** focuses on the effect of constant velocity motion on DIC uncertainty. This case is a simple condition of motion which can be applicable whenever the velocity change during the exposure time is negligible.
- **Chapter 4** on the other hand, investigates a more complicated motion low i.e. sinusoidal vibration. It is an important condition because of two main reasons. First, sinusoidal vibration is a quite common motion law in mechanical systems and therefore quantifying the displacement and strain of such a system could be of a great importance. Second, motion vibration is a dynamic case which is easy to be created in the laboratory. In this way the simulations could be validated by conducting harmonic vibration tests.

- In **Chapter 5**, DIC measurement uncertainty in dynamic conditions is evaluated by an experimental approach.
- In **Chapter 6**, a numerical technique to estimate the motion effect present in an acquired image is proposed. This numerical method is then implemented to improve the DIC uncertainty in dynamic conditions.
- **Chapter 7** contains the conclusion of the study and suggestions for future works.

CHAPTER 2

State of the Art

Studying the uncertainty of DIC in static applications started early on and remarkable advances have been made in this area especially in the recent years. In 2002, Hubert W. Schreier and Michael A. Sutton [4], analyzed the systematic error that arises from the use of under matched shape function, i.e., shape functions of lower order than the actual displacement field. They showed that, under certain conditions, the shape functions used can be approximated by a Savitzky-Golay low-pass filter applied to the displacement functions, permitting a convenient error analysis. They also claimed that, this analysis is not limited to the displacements, but naturally extends to the higher-order terms included in the shape functions and therefore permits a direct analysis of the systematic strain errors associated with an under matched shape function.

Later on, Thorsten Siebert, Thomas Becker et. al (2007) [5], investigated the impact of imaging system calibration errors by performing some tests in both static and dynamic applications. They presented a 3-D DIC system that provides online error information concerning diverse error sources and also the propagation of errors throughout the calculations to the resulting contours, displacements and strains. In the same year, V. Tiwari, M.A. Sutton et.al (2007)[6], obtained the effect of image distortions type on variability and accuracy of ultra high-speed and moderate speed image acquisition when employed in either 2D or 3D computer vision systems for deformation and shape measurements. Their baseline uniaxial tension experiments demonstrated that image correlation measurements using high speed imaging systems are unbiased and consistent with independent deformation measurements over the same length scale, with point-to-point strain variations that are similar to results obtained from translation experiments. In another study, Gi Jeung Um and Hyoung-Jin Kim (2007) [7], experimentally obtained the correlation error distributions around the hole in a paper tensile specimen at three different load levels.

A year later, H. Haddadi, S. Belhabib (2008) [8], proposed numerical and experimental tests, based on rigid-body motion in order to quickly assess the errors related to lighting, the optical lens (distortion), the CCD sensor, the out-of-plane displacement, the speckle pattern, the grid pitch, the size of the subset and the correlation algorithm.

In 2009, M. Bornert, F. Brémand, et.al [1], published a study on displacement error assessment from synthetic speckle images. Series of synthetic reference and deformed images with random patterns have been generated, assuming a sinusoidal displacement field with various frequencies and amplitudes. Displacements are evaluated by several DIC packages. Evaluated displacements are compared with the exact imposed values and errors are statistically analyzed. Their Results showed the general trends, rather independent of the implementations but strongly correlated with the assumptions of the underlying algorithms. They discussed various error regimes caused by parameters such as subset size, gray level interpolation or shape functions. In the same year, Bing Pan, Kemao Qianb et al. (2009) [9], Underlined the fact that some aspects of DIC, like the speckle patterns, which influence the accuracy and precision of displacement measurement have not been thoroughly investigated. Therefore, they derived a concise theoretical model, which indicates that the speckle pattern does not introduce systematic error but introduce random error in the measured displacement. Their Numerical experiments (with five speckle patterns with distinctly different intensity distribution taken from actual experiments) reached them to this conclusion that the standard deviation error of measured displacement are closely related to the speckle patterns and is in good agreement with the prediction of the proposed theoretical model.

Jakson M. Vassolera and Eduardo A. Fancelloa (2010) [10], claimed that almost all of the studies on accuracy and precision of DIC method, have been focused on the measurement errors for low order displacement fields, like translation and constant strain, and only a few works have been studied the error related to high-order displacement fields. Therefore, they investigated the displacement measurement accuracy for different possible sets of the DIC algorithm using numerically simulated images for zero, first and second order displacement fields in order to consider only errors related to the algorithm. They concluded that the accuracy may vary in many orders of magnitude from the choice of different setups, where the relation between the subset size and the speckle granule size is quite important.

M. Fazzini, S.Mistou (2010) [11], characterized a commercial software in order to estimate errors related to (DIC) technique applied to measurements of displacement based on the generation of synthetic images by which various parameters are treated, in order to determine their impact on the measurement error. These parameters are related to

the type of deformation imposed on the speckle, the speckle itself (encoding of the image and image saturation) or the subset size. In 2011, Zhenxing Hu, Huimin Xie et.al [12], presented a technique that evaluated the errors of the configuration, once 3D DIC system is set up and images of objects with speckles and calibration boards are recorded. They also theoretically analyzed the influence of the system calibration and image correlation on the error.

- **Theoretical Estimation of DIC uncertainty**

Some efforts have been made to theoretically estimate the DIC uncertainty [13]. In 2007, Z.Y. Wang, H.Q. Li et al (2007) [14], proposed a method to estimate the DIC error caused by intensity pattern noise. They presented a formula that synthetically reflects the effects of the variance of noise, the intensity variance and the subset size on the displacement measurement precision and verified the correctness of the resulting formula, by conducting two experiments. The first one was a real self-correlation experiment that aimed to analyze the effect of the subset size, while the second one was a numerical self-correlation experiment for analyzing the effect of the different noise levels.

In 2009, Phillip L. Reu, Michael Sutton et.al [15], quantitatively calculated the errors which will result from any given set of real images obtained in an experiment and concluded that the bias errors can be minimized by (a) selecting higher ordered shape functions, (b) increasing image contrast, and (c) selecting a subset with adequate information content and suggested that the variance parameter can be minimized by decreasing intensity noise in the images which can be accomplished either through better imaging equipment, improved illumination, lower camera gain, or by averaging multiple images at each step. They underlined the fact that both the bias and the variance strongly depend on the image gradients. In the same year, Y.Q. Wang, M.A. Sutton et.al [16], presented theoretical formulae defining the effect of noise in the intensity pattern, image contrast and interpolation method on both bias and variability in one-dimensional motion measurements.

In another study in 2009, Y. Q. Wang, M. A. Sutton et. al [17], obtained the expectation (bias) and variance in image motions in the presence of uncorrelated Gaussian intensity noise for each pixel location, by optimizing a least squares intensity matching metric. They quantified both the bias and the covariance matrix in 1D and 2D image analyses for image motion estimates as a function of: (a) interpolation method, (b) sub-pixel motion,

(c) intensity noise, (d) contrast, (e) level of uniaxial normal strain and (f) subset size. Their theoretical results in both cases of 1D and 2D showed that the expectations for the local parameters are biased and a function of: (a) the interpolation difference between the translated and reference images, (b) magnitude of white noise, (c) decimal part of the motion and (d) intensity pattern gradients.

Finally, Y.-Q. Wang & M.A. Sutton et.al. (2011) [18], used the basic equations for stereo-vision with established procedures for camera calibration, to provide the error propagation equations that can be used to determine both bias and variability in a general 3D position. They demonstrated that the general formulae provide a robust framework for quantifying the effects of various stereo-vision parameters and image-plane matching procedures on both the bias and variance in an estimated 3D object position. In the next step, they compared a series of stereo vision experiments' results such as uncertainty margins of the image locations/displacements, 3-D locations/displacements and strains with the theoretical predictions [19].

- **Implementing DIC in Dynamic Applications**

Although, the above mentioned works concerned static cases, the implementation of DIC did not remain limited to static applications. In 2003, T. Schmidt, J. Tyson et al. [20, 21], implemented advanced 3D image correlation photogrammetry in two dynamic applications. The first application aimed to utilize short-duration white light pulses for studying the automobile tires on road wheels at speeds up to 240 km/h and the second one was an initial work with a pulsed laser to study a flywheel in a spin pit at up to 35,000 rpm. Later on, Madhu S. Kirugulige, Hareesh V. Tippur (2007) [22], investigated the dynamic crack growth behavior of a polymeric beam that was subjected to impact loading using developed DIC methodology.

In 2009, Weizhuo Wang, John E Mottershead et al. [23], applied this method to the problem of mode shape recognition for a circular plate. In the same year, Thorsten Siebert, Rob Wood et al. [24], performed DIC approach for modal analysis and accurate full field measurements of displacement in three dynamic applications including harmonic vibration, shock phenomenon and noise excitation. In another work, the DIC technique was implemented in vibration analysis of a membrane, an impact test and an excitation of a circuit board using white noise [25].

In 2011, Weizhuo Wanga, John. E. Mottershead et. al [26] measured vibration mode shapes of a composite panel by a DIC analysis and used the results to modify and update

a FE model which predicts the structural responses. In another research, Mark N.Helfrick, Christopher Niezrecki et al.[27], provided a validation of DIC approach in vibration measurement by comparing the measured data using this method with the results obtained from accelerometers, scanning laser vibrometer and a finite element model. Finally in 2012, Weizhuo Wang, John E. Mottershead et al. [28], identified the modal properties of a car bonnet with 3D irregular shape by utilizing the domain-wise responses, captured by a DIC system and then compared the result with predictions of a FE model.

To the best of our knowledge, no researches have focused on systematic uncertainty assessment of Digital image correlation method in dynamic conditions, which is the aim of this work.

- **Implementing Finite Element Procedure**

In another interesting approach, group of studies implemented Finial element procedure to simulate the experiments. P. Lava, S.Cooreman et.al. (2009) [29], estimated DIC errors by using numerically deformed images that were obtained by imposing finite element (FE) displacement fields on an un deformed image yielding plastic deformation of the specimen, claiming that this FE procedure simulates realistic experimental heterogeneous deformations at various load steps. Using this method, the influence of the adopted correlation function, the interpolation order, the shape function and the subset size on the derived displacements was investigated. They demonstrated that DIC is able to reproduce these displacements up to a satisfactory level if conscious choices in the above-mentioned implementations are made. In another study in the next year, the same authors, focused on errors that can be directly attributed to the derivation of the strain fields, such as the strain-window size and the strain-window interpolation order using the same technique.[30]

In 2011, P. Lava, S.Coppieters et. al [31], in a study on the impact of a non-perpendicular camera alignment to a planar sheet metal specimen's surface, estimated errors by numerically rotating deformed images that were obtained by imposing finite element (FE) displacement fields on an un deformed image for various Euler angles. In the next year, Y. Wang, P. Lava et al.(2012) [32], by performing numerical 2D DIC tests on the deformation of numerically deformed images, taken from the real tensile specimens, found that the DIC accuracy and precision decrease under highly heterogeneous strain states. Their original images were deformed by imposed displacement fields, which were obtained by simulating uni-axial tensile tests of the

specimens with finite element analysis (FEA), claiming that in this way, the errors sourcing from the hardware of the image system are excluded. They also studied impacts of subset sizes, step sizes and strain window sizes for an optimum correlation.

- **Reference material for dynamic conditions**

Meanwhile, an interesting approach was followed by group of researchers aiming to establish a Reference Materials (RM) that can be used as an international standard to assess the uncertainty associated with a measurement system. E.A. Patterson, E. Hack (2007) [33], introduced a reference material and procedure for calibrating full-field optical systems suitable for measuring static, in-plane strain distributions. Efforts are now underway to extend this work and develop a reference material for calibration of systems capable of measuring three-dimensional deformation fields, induced by dynamic loading. [34, 35].

To the best of our knowledge, no researches have focused on systematic evaluation of DIC uncertainty in general dynamic applications, which is the aim of this work. In addition, here a numerical technique called deconvolution, is proposed which helps to decrease the bias error and the uncertainty of DIC measurements in dynamic conditions.

CHAPTER 3

DIC Uncertainty in the Case of Constant Velocity Motion

The current chapter focuses on DIC uncertainty assessment in the case of constant velocity motion. As it was mentioned earlier, this case is a simple condition of motion which is applicable whenever the velocity change during the exposure time is negligible. In order to analyze the uncertainty of DIC in any dynamic condition, a set of reference images of a target are required. In this chapter, two different methods to generate the image set is proposed and discussed in detail. First, in section 3.1 the issue of sub pixel shifting using Fourier Transform is addressed. This operation is required in the proposed methods for motion effect simulation (section 3.2, section 3.3 and section 3.5). The obtained image set is then used in order to evaluate the DIC uncertainty in the case of constant velocity motion (section 3.4). In section 3.6 performances of the two methods are compared.

3.1 Sub Pixel Shift Using DFT

Simulation of pure translation is the first step towards simulating the motion effect as will be explained in section 3.2. Different approaches were introduced in the literature for this matter. Fourier shifting is one of them that is claimed to be the optimum sub pixel shifting technique by P.L.Reu [36]. This technique is based on convolving the image with a shifted impulse function and is composed of three simple steps. The image is first transformed into the frequency domain via Discrete Fourier Transform (DFT). Then, a linear phase shift (i.e. with a phase shift linearly proportional to the spatial frequency) is applied in the complex plane. The amount of added phase determines the amount of the spatial shift. Finally the image is transformed back to the spatial domain via an inverse Fourier Transform. The transforms are done via 1D DFT of one row or one column at a time [36].

It is important to emphasize on the fact that the convolution of the image with a shifted impulse function in the spatial domain would allows us only to simulate integer pixel displacements and thus this shifting technique has been implemented in the frequency domain by Reu [36].

The reference images used in this work, were composed of an unfiltered and a filtered 400*400 pixels speckle pattern both having grain size of 4 pixels. Working on an unfiltered and a filtered reference image allows analyzing the DIC behavior on both very well-focused images (i.e. the basically theoretical images) and on slightly blurred ones (i.e. images with a blurring level that can simulate real acquisition conditions). Figure1 shows the reference images. The filtered image is obtained after filtering the unfiltered one by a low pass Gaussian filter with sigma=0.75.

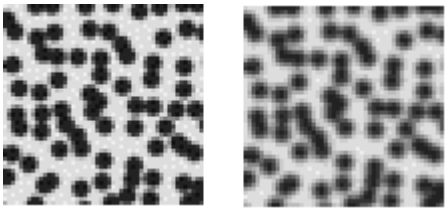

Figure 1. Part of the reference image before filtering (left) and after filtering with a low pass Gaussian filter with sigma=0.75 (right).

In order to check the performance of this sub pixel shifting method, the procedure explained above is preformed on the reference images shown in Figure 1, numerically simulating a rigid motion of the target from 0 to 8 pixels with a 0.1 pixel step. Figure 2 represents the result of Digital Image Correlation analysis performed on the generated images.

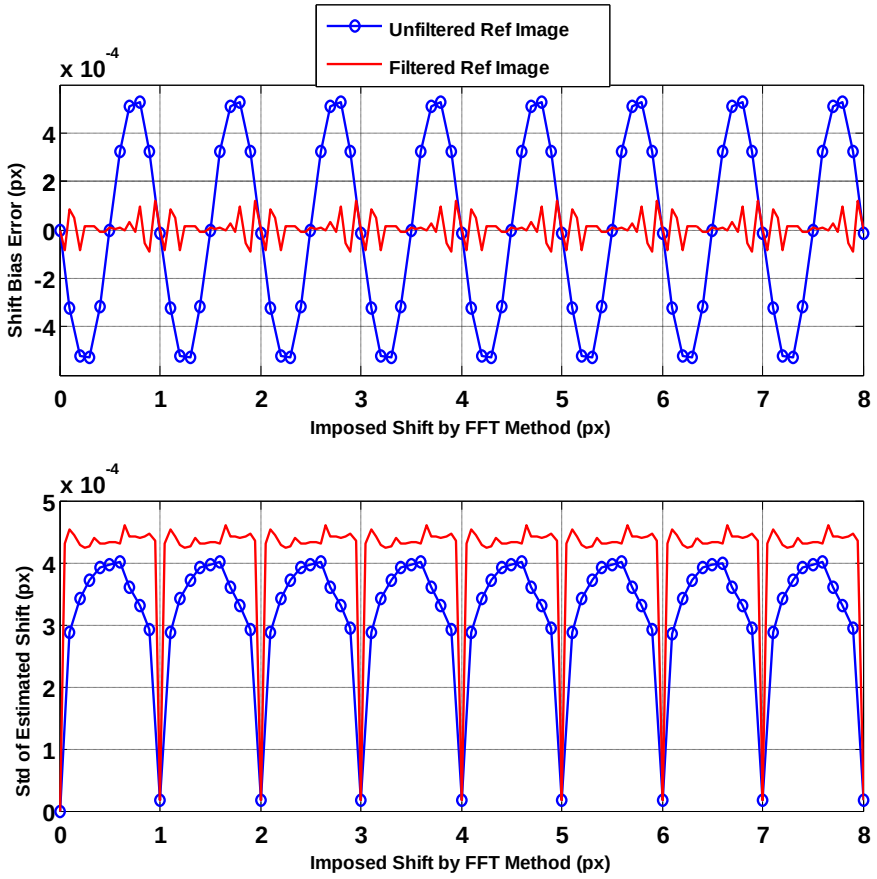

Figure 2. Evaluation of DFT sub pixel shifting method, Bias Error or simply u-u_ref (up) and standard deviation of estimated shift (down).

In Figure2, the Bias error i.e. the difference between the displacement estimated by DIC and the corresponding imposed shift value is shown versus the imposed rigid displacement. The sinusoidal trend in the case of unfiltered image (Figure 1a) has been noticed and recognized in the literature [13, 36, 37]. The amplitude of this systematic effect depends on subset size, blurring and the shift creating method itself. In this study, the chosen method for shifting is the optimum one [36] however; the other two factors are still present. According to Figure 2, applying the current method for generating shifted images introduces an uncertainty less than 0.001 pixels.

The shifting technique can therefore be used to develop the method to simulate the motion effect as described in section 3.2.

3.2 Generation of Images with Motion Effect

As it was already discussed in the last section, convolving the image with impulse function is a recognized method to simulate the sub pixel shifting. In order to generate images with motion effect two main techniques can be considered. The first technique is the square pulse method which is based on convolution of reference image with a square pulse (see section 3.3). The second one is the averaging method which will be introduced later in section 3.5. As it will be demonstrated later, in some dynamic cases the latter, better simulates the real conditions.

3.3 Motion Effect Simulation Using Square Pulse

As it was already discussed in section 3.2, convolving the image with impulse function is a recognized method to simulate the sub pixel shifting, considering that the position of the impulse peek determines the value of imposed shift. In the case of dynamic conditions, the motion of the target during the exposure time is often not negligible. This phenomenon causes a motion effect (i.e. blurring) on the acquired images. In this study we propose an innovative technique, capable to recreate on a given speckle pattern, both the displacement and the blurring effect due to the motion of the measurement surface. The generated images will be used to test the performances of DIC in dynamic conditions.

Figure 3 explains the approach using a simple example. A target is translating along the x axis and a frame is grabbed when the displacement is equal to 1 pixel. Under assumption of instantaneous acquisition, the acquired image would be just the same as the reference image but with a one pixel shift to the right and it can be simulated by convolving the reference image with the impulse function in Figure3(a). In this figure the impulse function is represented by G(x). Considering now the scene recorded by means of a real camera, a given time is required for the camera to grab the frame. In this example, the target displaces half of a pixel during this exposure time. In order to simulate the acquired image in this case, we suppose to generate several instantaneously acquired images during the exposure time and average them (Figure 3(b)). If we increase the number of intermediate images up to infinity, we would get a square pulse with a width equal to the target's displacement during the exposure time also called simply as the strip length.(Figure3(c)). Based on this explanation, we propose here a motion effect simulation technique, which involves convolution of image with square pulse.

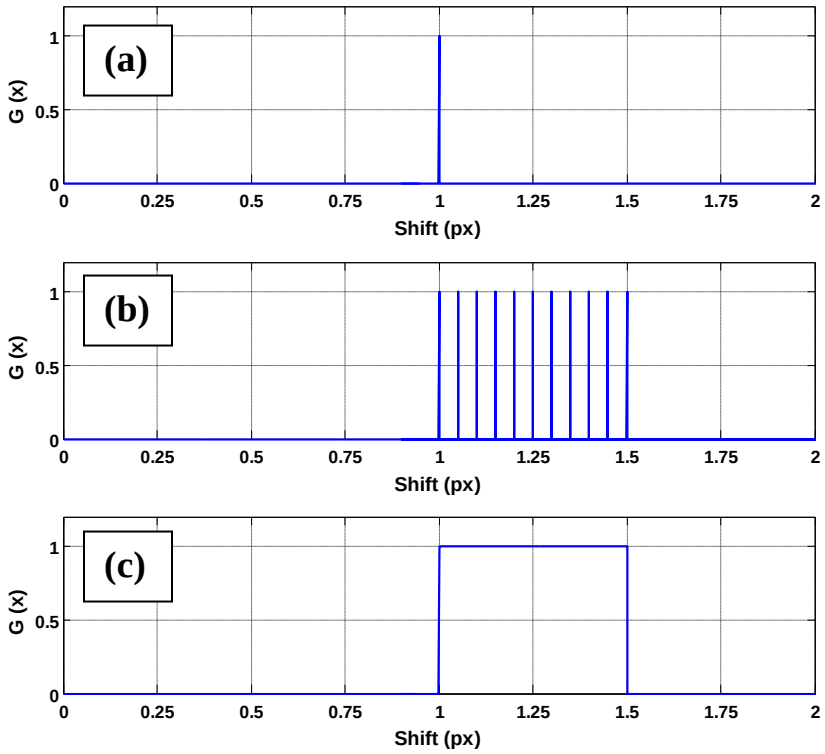

Figure 3. Simulation of motion effect
Generation of a shifted image using a shifted impulse function (a), generation of several intermediate images using the corresponding shifted impulse function (b), simulation of motion effect using a square pulse (c).

For explaining the square pulse motion effect simulation technique a brief review over the characteristics of square pulse and its Fourier transforms seems to be essential.

3.3.1 Square Pulse and It's Fourier Transform

The square (rectangular) pulse g(t), symmetric with respect to the time $t = 0$, can be defined as:

$$g(t) = rect\left({}^{t}/_{w}\right) = \begin{cases} 1 & \text{if } |t| < \dfrac{w}{2} \\ 0 & \text{if } |t| > \dfrac{w}{2} \end{cases} \qquad (1)$$

Index 'w' is the parameter which indicates the width of the rectangle (i.e. the length of the stripe generated on the image).

The Continuous Fourier transform of this function can be written as below [38]:

$$G(f) = \int_{-\infty}^{\infty} rect(t/w) e^{-j2\pi ft}\, dt = w\frac{\sin(w\pi f)}{w\pi f} = wsinc(wf) \qquad (2)$$

In the case of dealing with a shifted square pulse (not centered) the Fourier transform is calculated as below:

$$FT[\, g(t-a)] = FT[g(t)] * \exp(-2i\pi fa) \qquad (3)$$

Where 'a' represents the time shift of the square pulse.

According to Equation (2), the continuous Fourier transform of a square pulse is a sinc function. It is important to point out that, Discrete Fourier Transform of this pulse is not a sinc function, and can be obtained starting from the discrete definition of the square pulse in time domainX[n]:

$$\mathrm{X[n]} = \begin{cases} 1 & 0 < n \leq N \\ 0 & otherwise \end{cases} \qquad (4)$$

DFT of the discrete Square pulse X[n] in [38]:

$$\mathrm{X}\,(e^{j\omega}) = \sum_{-\infty}^{\infty} \mathrm{X[n]}\, e^{-jn\omega} = \sum_{n=0}^{N-1} \mathrm{X[n]}\, e^{-jn\omega} = \frac{1-(e^{-Nj\omega})}{1-e^{j\omega}} = e^{-\frac{j\omega\,(N-1)}{2}} * \frac{\sin\left(\frac{\omega N}{2}\right)}{\sin\left(\frac{\omega}{2}\right)} \qquad (5)$$

Figure 4, represents a Square pulse signal with unitary width (w=1) and the corresponding Discrete and Continuous Fourier Transform. Discrete and continuous Fourier transform of the square pulse will be used in the next subsections to simulate the motion effect.(see section 3.3.2 and section 3.3.3)

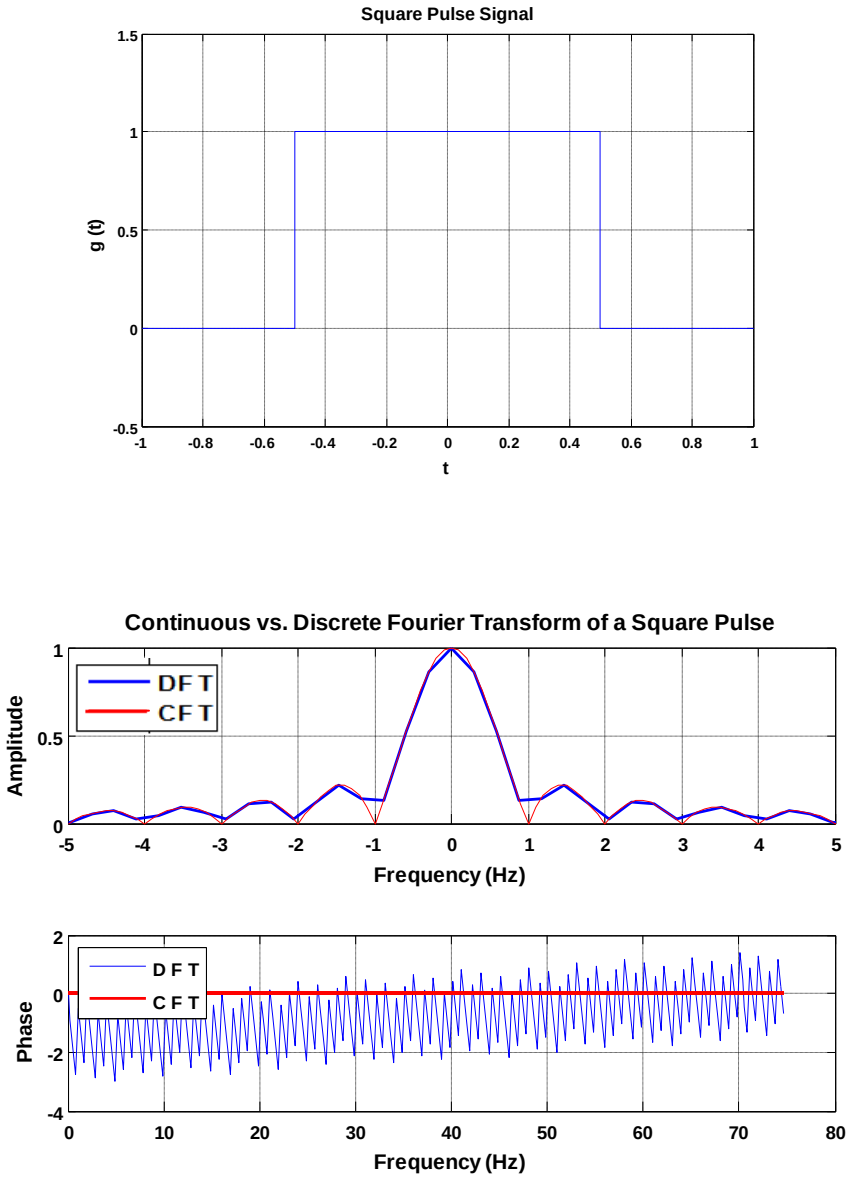

Figure 4. A Square pulse with w=1 (up) and corresponding Continues and Discrete Fourier Transforms (down).

3.3.2 Numerical Method for Motion Effect Simulation Using Square Pulse

According to the convolution theorem, the convolution in space domain is equivalent to multiplication in spatial frequency domain. The proposed technique to simulate the motion effect in horizontal direction is to calculate the DFT of each row of the image and multiply it by DFT of square pulse and finally calculate the inverse DFT of the product. Analogous procedure can be done operating with image columns to simulate a vertical motion effect. We call this procedure, **Numerical Method of motion effect simulation.**

It should be mentioned that if we convolve the image with shifted square pulse in space domain we will get a shifted image with motion effect.

3.3.3 Analytical Method for Motion Effect Simulation Using Square Pulse

The limitation for using the numerical method is that, the square pulse length value can only accept the integer values but there is a need to simulate the motion with sub-pixel accuracy. Therefore the **Analytical Method** is proposed. Analytical method is based on creating the Fourier transform of the square pulse directly in frequency domain without the need to work in space domain; this will allow handling also motion effect with sub-pixel amplitude. The continuous Fourier transform of square pulse (i.e. Sinc function) is directly multiplied by the DFT of each row of the reference image and the inverse DFT of the product is computed. An important issue regarding implementation of this method is to correctly define the frequency domain based on oddity or evenity of the signal length which has been addressed previously by P.L.Reu [36].

3.3.4 Numerical Issues Related to Motion Effect Simulation

Applying either of the two mentioned methods (Analytical or Numerical) on an image with an area containing sharp intensity changes might make the generated image to have periodic intensity changes in that same area, Figure5.

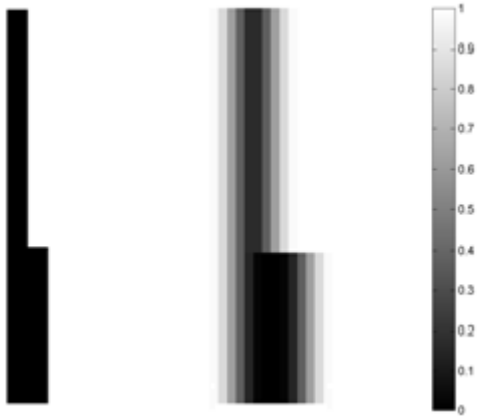

Figure 5. An image with sudden intensity changes (left) and the corresponding generated image which has a periodic intensity behavior (right).

The reason could be explained with the Shanon theorem. According to this theorem we cannot measure the part of frequency content which is higher than half of sampling frequency. Figure 6 represents what happens when we sample a signal (an image row or column) with a sharp change in intensity. As the intensity changes in the signal is smoothened (Figure6, right) the periodic behavior would be less visible in the reconstructed signal.

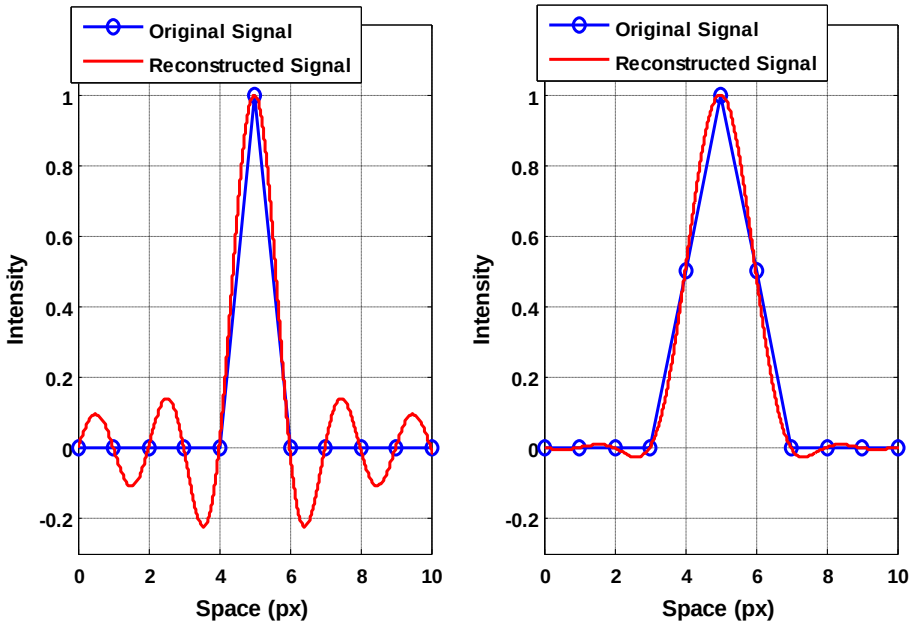

Figure 6. Sampling a reference signal with a sharp change in intensity. Left figure shows better approximation (less periodic behavior) since the changes in original signal is smoother.

In the case of usual DIC speckle patterns, this sharp intensity changes are not significant. Moreover, camera basically performs as a low pass filter which smoothes these rapid changes. Therefore this negative effect is barely visible in the case of this work and could be neglected.

3.3. 5 Generation of Images with Constant Velocity Motion Effect Using the Square Pulse

In order to apply the square pulse method the only concern is to obtain the equivalent shift and width of the square pulse corresponding to the motion or in the other words, to

define values of parameters ‘w’ and ‘a’ in equations (2) and (3). In the case of rigid motion, parameter ‘a’ can be easily defined since it represents the net displacement of the target with respect to the reference image. This value is equal to zero. On the other hand ‘w’, is the length of the path covered by the target during an exposure time. For a given set of ‘w’ and ‘a’ parameters, the procedure explained in section 3.3.3, can be readily implemented.

3.4 DIC Uncertainty Assessment Using Square Pulse Technique, Constant Velocity

This section starts with DIC analysis of numerically generated images with motion effect (section 3.4.1). Then the effect of adding noise to this group of images is investigated (section 3.4.2). Next, the acquired images of sinusoidal vibration in few cases were simulated by the proposed technique and the uncertainties of the measurements were estimated using DIC analysis. In order to validate the model, the results of experiments were compared with that of the simulations (section 3.4.3).

3.4.1 DIC Analysis of Images with Constant Motion Effect

In the current study Vic-2D software is used in order to perform the DIC analysis. The subset size and overlap were set equal to 21 and 7 pixels respectively [39]. Figure7 illustrates the generated images with an increasing motion effect w in the case of rigid motion.

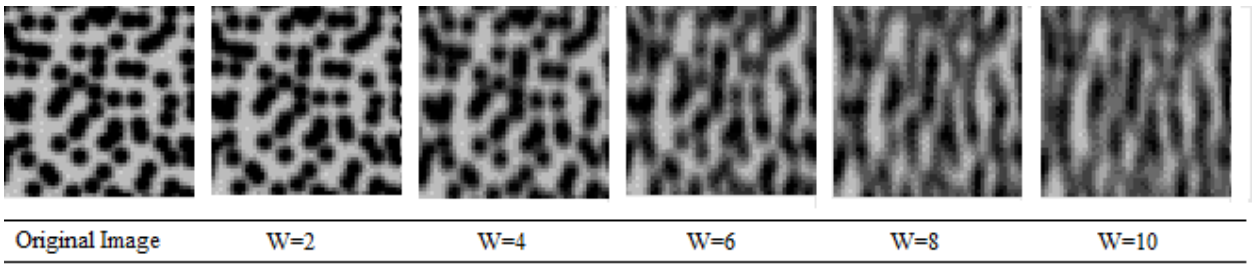

Figure 7. Sense of motion effect as the index w increases in the generated image.

By performing DIC analysis on the generated images with respect to the original one the displacement and strain value of every subset was obtained. These values have been computed over the whole image and the result is reported in Figure8, in terms of mean and standard deviation of the discrepancy between the imposed and estimated motion. In Figure 8 only the result for $w \leq 8$, is shown because the Digital Image Correlation method is barely able to detect the pixels in the generated image with w index higher than 8.

At first (results shown in Figure 8), the reference displacement has been set equal to zero in both horizontal and vertical directions and motion effect i.e. blurring, has been applied along the vertical direction. The discrepancy standard deviation can be noticed to be about one order of magnitude bigger than the discrepancy average and it can consequently been considered a reliable estimation of the measurement uncertainty. Therefore, it can be claimed that the uncertainty is the meaningful quantity (not mean) that should be taken into account. According to Figure 8, in all cases it increases faster as 'w' increases.

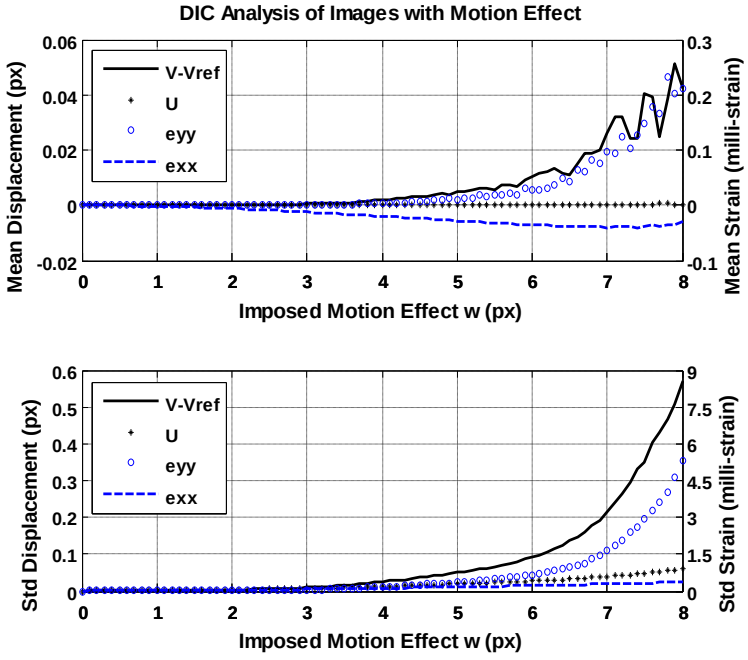

Figure 8. Mean and standard deviation of displacement and strain in the case of constant velocity motion with zero displacement (V and eyy are respectively the displacement and strain in the direction of Motion. U and exx are displacement and strain in the opposite direction).

In order to investigate DIC performances in the case of rigid motion when the net displacement is not equal to zero, sub pixel shifting method, discussed in section 3.1, is applied on the two reference images shown in Figure 1. Figure 9, represents the results in the case of shifting an image with an imposed motion effect of w=7 (to simulate a condition of a strong motion effect).

According to this figure, bias error and standard deviation of the estimated shift both show an overall constant trend with small fluctuations around their corresponding value obtained in the case of zero displacement (Figure 8). This can prove that the uncertainty of result mainly depends on the motion effect while the shifting value has a negligible effect. Due to the simulated motion effect (w=7), both the bias and the standard deviation of the shift shown in Figure 9, are much larger than the corresponding ones shown in Figure 2.

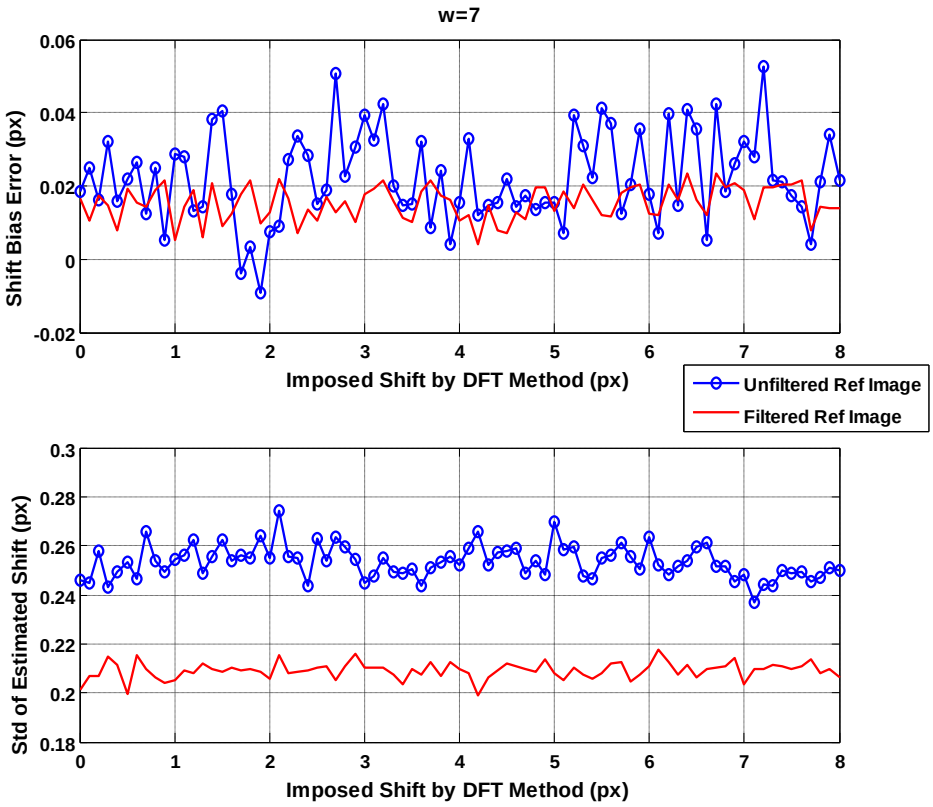

Figure 9. DIC results in the case of constant velocity motion and non-zero displacement.

3.4.2 Effect of Adding Gaussian Noise to the Generated Images

In this subsection a Gaussian noise in two levels was added to the generated images before applying the DIC analysis in order to check if this, changes the uncertainty in some way. Figure 10, shows the mean and standard deviation of displacement and strain after adding noise to the images. Noise level1 and level2 are two zero mean Gaussian noises with standard deviation of 5 and 10 respectively. The reference displacement is equal to zero in both horizontal and vertical directions but the motion effect (stripe) is simulated in vertical direction. Comparing Figure10 with Figure8 demonstrates that adding Gaussian noise to the image cannot significantly affect neither the mean values, nor the uncertainty.

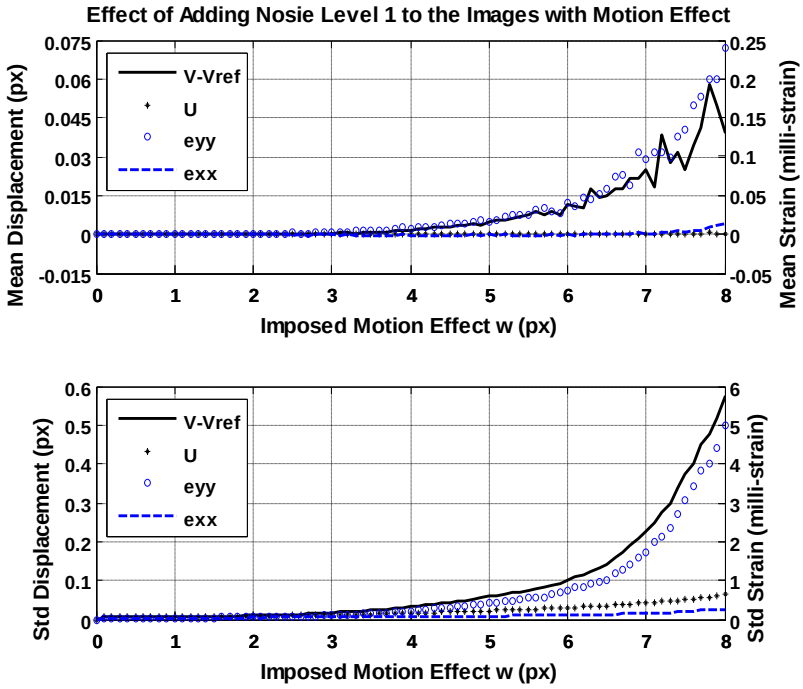

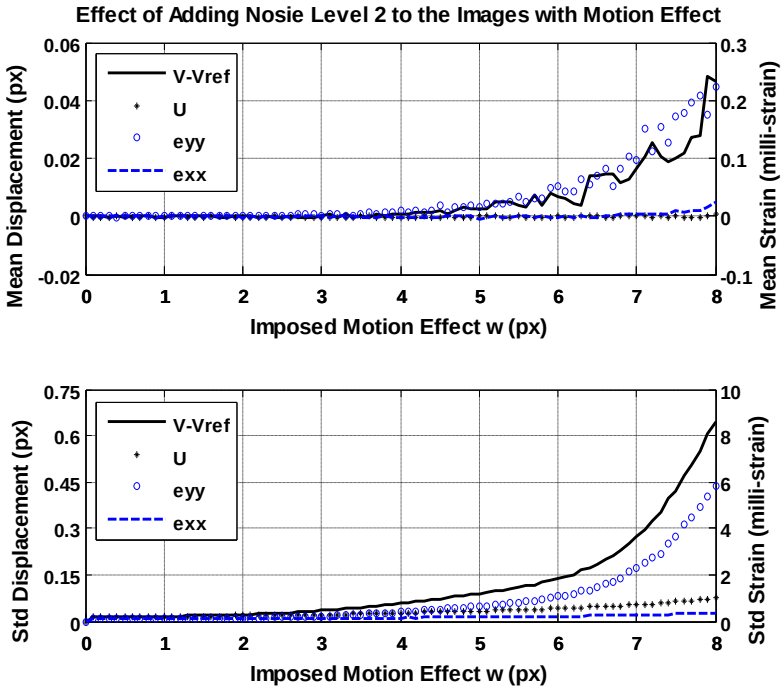

Figure 10. Mean and standard deviation of displacement in the case of constant velocity motion after adding noise with level one (up) and with level two (down) (V and eyy are respectively the displacement and strain in the direction of Motion. U and exx are displacement and strain in the opposite direction).

3.4.3 Analytical SSD Analysis of Images with Rigid Motion Effect

It is important to find out the main sources of uncertainty in the results, reported in pervious subsections (section 3.4.1 and section 3.4.2). Up to now both the image quality (due to the motion effect) and the DIC technique could be the possible source of the uncertainty. In the other words, we need to determine whether it is the DIC which is unable to reliably estimate the displacement in the case of motion effect in the images or if the images with motion effect do not allow the image processing technique to have a reliable estimation. In order to find the correct explanation, a different image processing technique (a two dimensional Sum of Squared Differences (SSD) analysis [40]) is used here to analyze the generated images. In contrary to DIC, which is a very flexible method that works with deformable subsets, SSD is a very constrained technique that allows only rigid translations. Moreover because of the fact that the strain is a derivative of displacement it is important to validate the displacement result obtained by DIC method.

Since the goal of this analysis was to check the results of DIC, every condition had to be set similar to that analysis. Therefore, the subset was set to 21*21 pixels with overlap of 7 pixels the same as before.

In order to increase the resolution of SSD computations to sub pixel resolution, it is important to up sample the generated images. In this work, the 2D interpolating method using Discrete Fourier Transform was implemented for up sampling. This is a popular method used also to improve DFT spectral estimation, known as zero padding in frequency domain. This process involves adding zero-valued data samples to an original DFT input sequence and performing an inverse DFT on this new signal in order to increase the total number of input data samples [41]. The main advantage of this technique, apart from it's simplicity, is the fact that the 2D Fast Fourier Transform of the original image remains unchanged after interpolation. Further computational details are available in [41, 42].

The procedure was basically to perform the SSD analysis over the whole image, in order to find the mean and standard deviation of displacement in horizontal and vertical direction. Figure11 shows the result with 10 times up sampling. In this figure, the discrepancy standard deviation is about two orders of magnitude bigger than the discrepancy mean and therefore can be considered a reliable estimation of the measurement uncertainty (same thing as the case of DIC, Figure8).

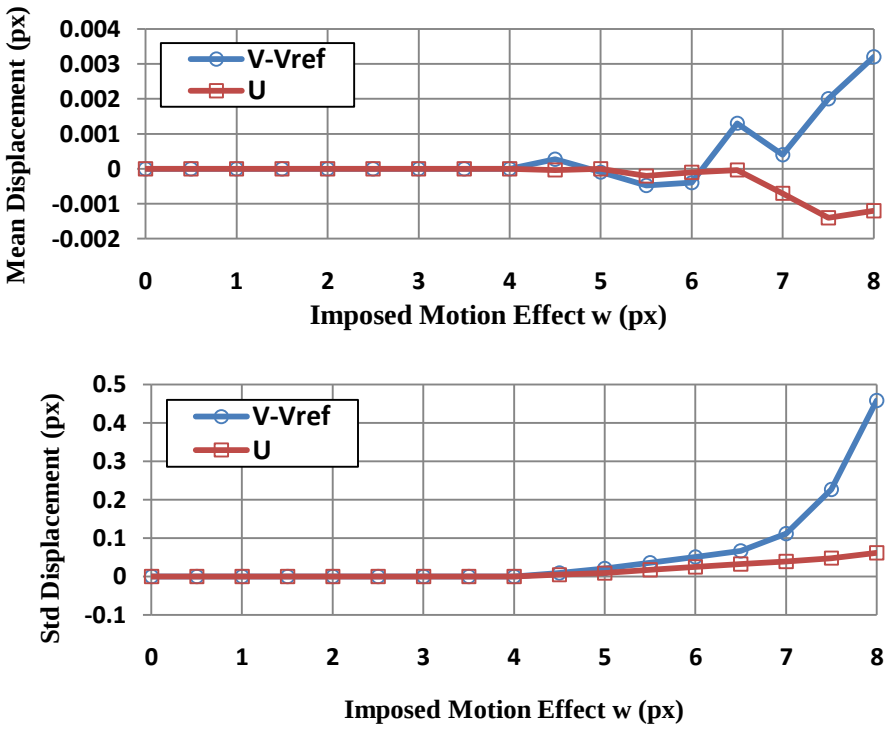

Figure 11. Mean (up) and standard deviation (down) of displacement using 2D_SSD analysis with upsampling factor=10 in the case of constant velocity motion.

The displacement standard deviation curves in Figure 11 are in a good agreement with the corresponding ones in Figure 8 and can prove that the uncertainty in the estimation of displacement in the case of DIC (Figure 8) is not due to the image processing technique itself but is due to the presence of motion effect in the generated images.

3.5 Motion Effect Simulation by Averaging the Shifted Images

The square pulse simulation technique works better when the velocity of motion can be assumed constant during the exposure time. It is due to the shape of the square pulse, which is constant over its width. In the cases in which this hypothesis (constant velocity during the exposure time) is not valid, we suggest to implement the second technique, averaging. As an example in the case of sinusoidal motion, we expect the averaging approach to simulate the reality much better than the square pulse method. The reason is that when the object is close to the peeks the velocity considerably changes. Moreover, the averaging method is simple and based on the approved method of FFT shift [36].

3.5.1 Generation of Images with Constant Velocity Motion Effect Using the Averaging Technique

In the case of rigid motion, both methods are applicable if the velocity is considered to be constant. Applying averaging method is even more straightforward than square pulse method. The procedure is consisted of two steps. First step is to generate 'N' shifted images during the exposure time, each being displaced by 'a_j' pixel in respect to the reference image. In which 'a_j' is the shift value in pixels. In the case of zero displacement this value can be obtained from the equation below:

Shift value (px): $$a_j = -\frac{w}{2} : \frac{w}{N} : \frac{w}{2} \qquad (6)$$

In which 'w', is the length of the path covered by the target during the exposure time and 'N' is number of samples. The second step is to average these generated images and obtain a single image. This image is the simulated version of the real image, of the target. By increasing the number of the samples 'N', we will have better estimation of the average image.

3.6 Comparison of the Two Motion Effect Simulation Technique, Constant Velocity

In the current section, the results of the two simulation methods are compared in the case of constant velocity rigid motion. In order to compare the two methods of motion effect simulation in the case of rigid motion with constant velocity, DIC analysis on these two groups of images was performed and the results in terms of estimated displacement and strain were compared.

By performing DIC analysis on the generated images the displacement and strain value of every subset was obtained. These values have been averaged over the whole image and the result is reported in Figure12 and Figure 13, in terms of mean and standard deviation of the discrepancy between the imposed and estimated motion. In these figures only the result related to $w \leq 8$, is shown because the Digital Image Correlation method is barely able to detect the pixels in the generated image with w index higher than 8.

In the case of results shown in Figure 12 and Figure 13, the reference displacement is equal to zero in both horizontal and vertical directions but since the motion effect (stripe) is simulated in vertical direction, the estimated values of displacement and strain are higher in this direction. Uncertainty values of all four parameters (U, V, exx, eyy) are considerably higher than their corresponding mean. Therefore, it can be claimed that the uncertainty is the meaningful quantity (not mean) that should be taken into account. In addition, up to w=4px, displacement uncertainty is negligible. Then it starts increasing with an almost constant slope (4px<w<6px) and as we pass w=6px the growth rate rises considerably fast. (Figure12). Strain uncertainty curve show similar behavior (Figure13).

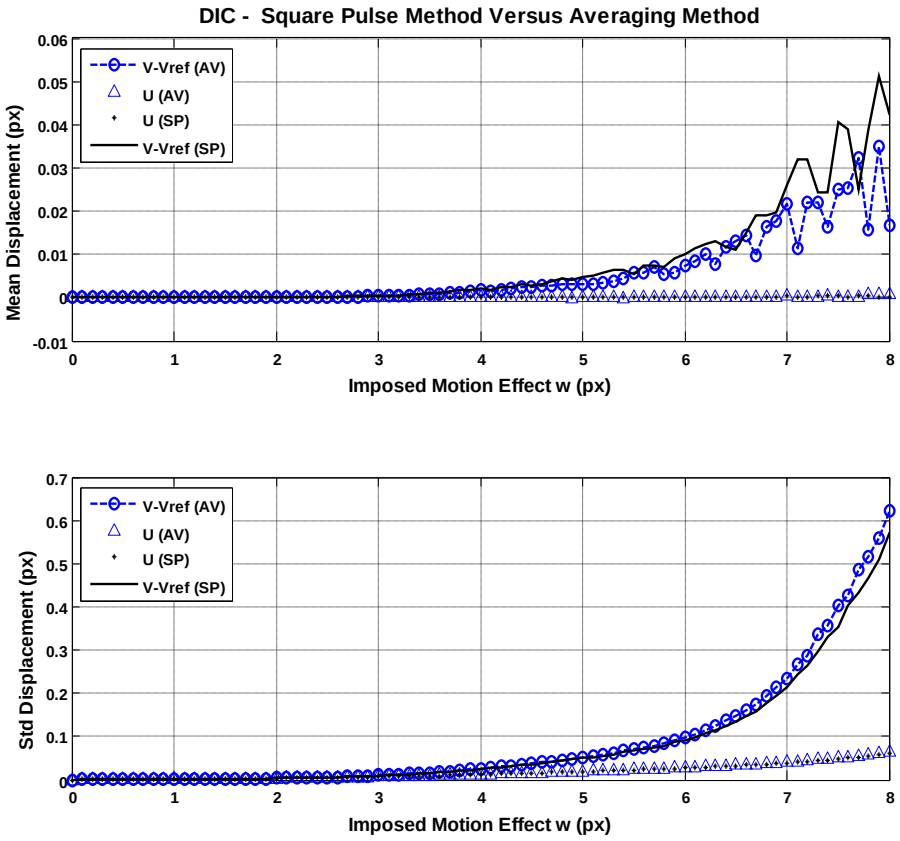

Figure 12. Mean and standard deviation of Displacement in the case of constant velocity motion simulation. V is the displacement in the direction of Motion and V_ref=0. While U, is displacement in the opposite direction. 'AV' represents the averaging method and 'SP' represents the square pulse method.

Figure 12 and Figure 13, demonstrate that in the case of simulating rigid motion with constant velocity there is no considerable difference between estimated displacement and strain by the two methods.

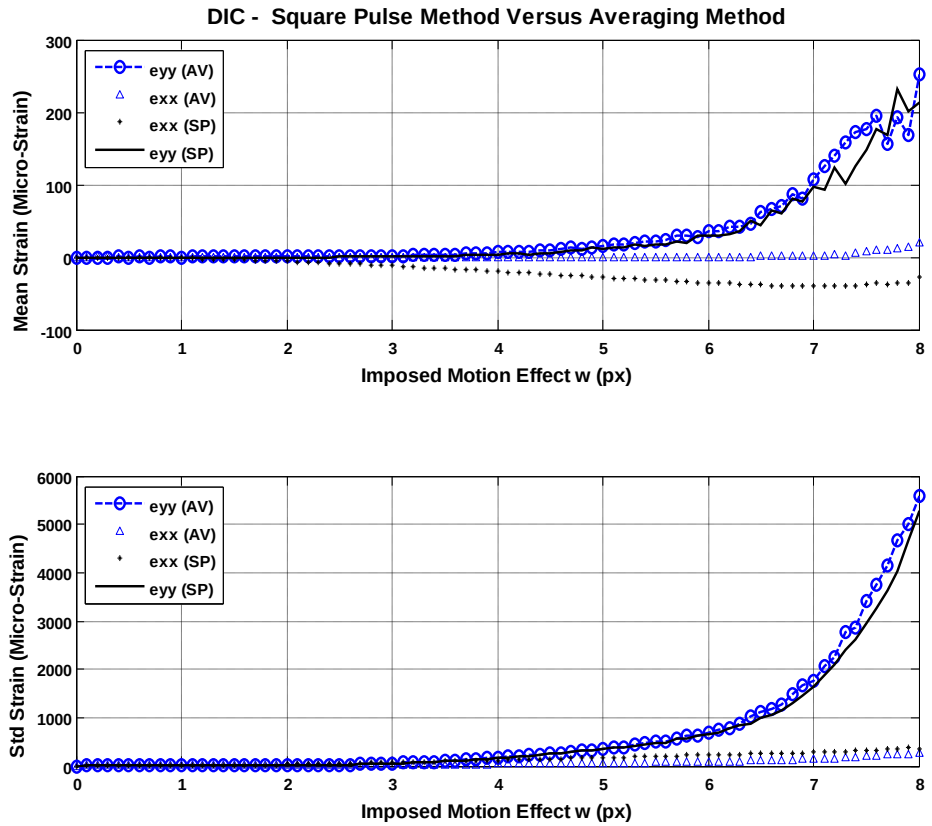

Figure 13. Mean and standard deviation of strain in the case of constant velocity motion simulation. eyy is the strain in the direction of Motion. While U, is the strain in the opposite direction. 'AV' and 'SP' respectively represent the averaging method and the square pulse method.

CHAPTER 4

DIC Uncertainty in the Case of Sinusoidal Vibration

The current chapter focuses on DIC uncertainty assessment in the case of sinusoidal vibration. As it was mentioned earlier it is an important condition because of two main reasons. First, sinusoidal vibration is a quite common motion law in mechanical systems and therefore quantifying the displacement and strain of such a system could be of a great importance. Second, motion vibration is a dynamic case which is easy to be created in the laboratory. In this way the simulations could be validated by conducting harmonic vibration tests. In order to analyze the uncertainty of DIC in any dynamic condition, a set of reference images of a target are required. In this chapter, the two motion effect simulation methods are used to generate the image set according to the motion displacement law (section 4.1 and section 4.2). The obtained image sets are then used in order to evaluate the DIC uncertainty in the case of sinusoidal vibration and the corresponding results are validated by conducting few real tests (section 4.3).

4.1 Simulation of Acquired Images in a Sinusoidal Vibration Using the Square Pulse Technique

In this segment the proposed motion effect simulation method is implemented to simulate acquired images in the case of target moving with the sinusoidal vibration. The chosen speckle patterns are the ones previously presented in Figure 1. Figure 14 illustrates the implemented method to simulate i_{th} image. The acquisition of the i_{th} frame starts at $t=ti$ and ends at $t=ti+sh$, being sh an imposed shutter time of the camera. Assuming sh to be "small" with respect to the period of the sinusoidal waveform, the velocity within sh can

be approximately considered constant. Under this hypothesis, the displacement of the target can be expressed as:

$$\textit{Target's displacement:}\quad a = A\sin\left(\frac{2\pi}{T}\left(t_i + {sh}/{2}\right)\right) \qquad (7)$$

In which, A and T are respectively the amplitude (in millimeters) and the period of the displacement law (in seconds) and 'a' is the position of the target at $t = t_i + {sh}/{2}$(position at the middle of the exposure time), (Figure 14).

On the other hand the displacement of the target during sh quantifies the width of the square pulse (w) introduced in section [3.3.5]. It can be simply written as:

$$\textit{Equivalent width of square pulse}:\ w = A[\sin(\frac{2\pi}{T}(t_i + sh) - \sin\left(\frac{2\pi}{T}t_i\right)] \qquad (8)$$

Now before substituting the calculated value of 'a' and 'w' from equation (7) and (8) into equation (2) and (3) these values should be converted into pixels using the camera scale factor. (The aim of this part was to implement Analytical method of motion effect simulation; the reason of this choice has been already discussed in section 3.3.3).

It is worth to stress that the imposed displacement in the simulated image is equal to 'a', i.e. displacement of the target at $t = t_i + {sh}/{2}$ (displacement at the middle of the exposure time).

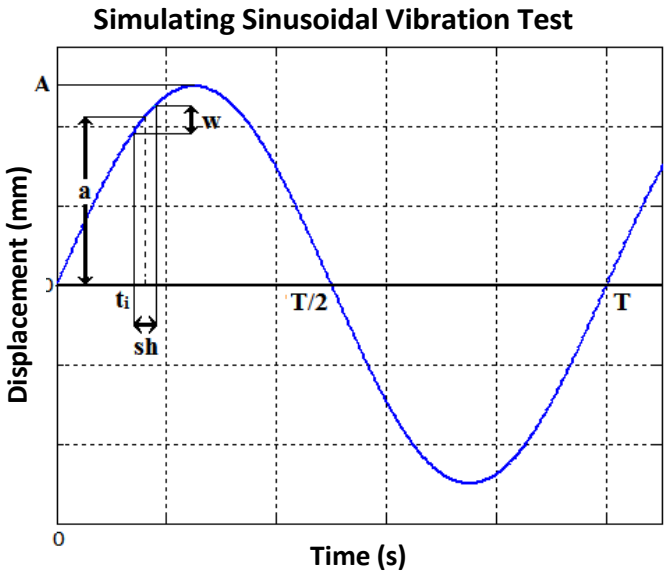

Figure 14. Simulating the sinusoidal vibration test (Square Pulse).
Parameters 'A' and 'T' represent amplitude and period of the sinusoidal displacement law. Acquisition starts at $t=t_i$ and ends 'sh' (exposure time) seconds later at $t= sh+t_i$. Parameters 'a' and 'w' are considered as values of shift and motion effect index in generation of corresponding simulated image.

Consequently, once the sampling frequency of the image acquisition hardware and its shutter time are defined, it is possible, for a given sinusoidal motion law, to numerically generate a sequence of frames as expected to be captured by the camera starting from a single image of the speckle pattern acquired in static condition.

4.2 Simulation of Acquired Images in a Sinusoidal Vibration Using the Averaging Technique

As it was discussed earlier, in the case of sinusoidal vibration, velocity changes, during an exposure time is not negligible. The case is even worse if we are dealing with longer exposure time in respect to the period of harmonic displacement law. Therefore in such conditions, the averaging method is expected to be more reliable than the square pulse method. Later on, in section 4.3 we will demonstrate this statement.

Figure 15, helps to understand how the averaging method is implemented in order to simulate i_{th} image, acquired at $t = t_i$. This acquisition takes 'sh' seconds and ends at

$t = t_i + sh$, in which 'sh' represents the exposure time (shutter time). First step of simulation is to generate 'N' shifted images during the exposure time, each having a shift value calculated as below:

Object's displacement: $a_j = A\,sin\left(\frac{2\pi}{T}(t_j)\right)$ (9)

In which: $t_j = t_i + j * \left(sh/N\right)$ (10)

Index 'j', represents the j_{th} shifted image in the interval (exposure time). A and T are respectively the amplitude (in millimeters) and the period of the displacement law (in seconds) and 'a_j' is the displacement of the object at $t = t_j$, (Figure 15).

Next step of simulation is simply to average these generated images in order to get the i_{th} simulated image. Again here, by increasing the number of the samples 'N', we will have better estimation of the average image.

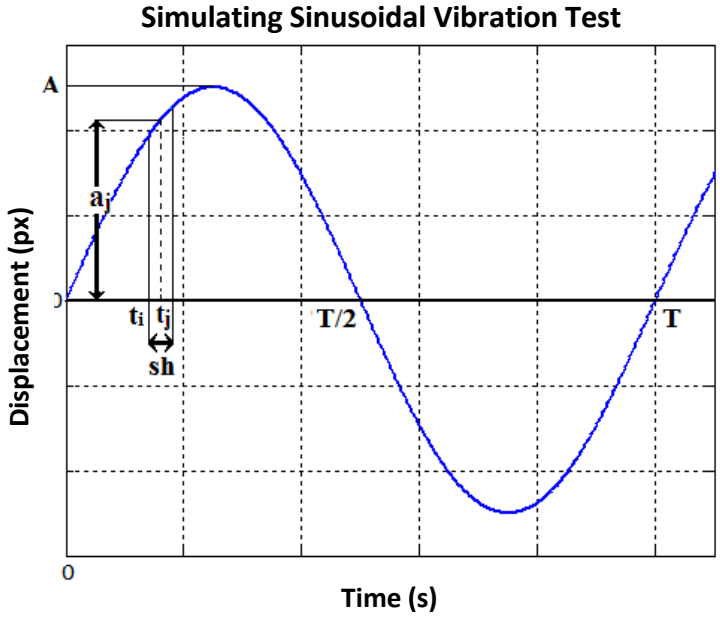

Figure 15. Simulating the sinusoidal vibration test (Averaging).
Parameters 'A' and 'T' represent amplitude and period of the sinusoidal displacement law. Acquisition starts at $t=t_i$ and ends 'sh' (exposure time) seconds later at $t= sh+t_i$. Parameter 'a_j' is the shift value used to generate one of the shifted images during the exposure time at 't_j' is the corresponding time.

4.3 Comparison of the Two Motion Effect Simulation Technique, Sinusoidal Vibration

In this section, the two proposed simulation techniques were implemented on the planar target with sinusoidal vibration. The procedure of image generation is already revealed in section 4.1 and section 4.2. As the next step, the simulated image set is analyzed with the DIC technique. Table 1, represents the specifications of the simulated sinusoidal vibration cases. These sinusoidal tests were conducted also in the laboratory, in order to validate the simulations (see section 4.3.1). The last column is the 'maximum nominal stripe length' which can be defined as is the length that the object displaces during an exposure time (or simply the strip length) if it has the maximum speed the whole interval. It is calculated as below:

$$Max\ Nominal\ Stripe\ Length = Max\ speed * sh = 2\pi f A * sh \qquad (11)$$

In which, 'f' and 'A' are respectively the nominal frequency (in hertz) and amplitude (in millimeters) of the specific test and 'sh' is the exposure time (shutter time in seconds).

Table 1. Specifications of simulated tests

Test Number	Amplitude (px)	Frequency (Hz)	Exposure Time (ms)	Frame Rate (Frame/s)	$\frac{(\text{Eposure time(s)})}{(\text{Period(s)})}$	Max Nominal Strip Length (px)
1	1.5	5	4	20	0.02	0.1881
2	9	5	5	20	0.025	1.4104
3	9	5	20	20	0.05	5.6417
4	15	5	15	20	0.075	7.0521
5	21	15	4	16	0.06	7.8983

Aiming to recreate the conditions of real tests a zero mean Gaussian noises with standard deviation of 2.5 was added to the images.

4.3.1 Experimental Validation

In order to validate the results of simulations, the simulated cases were also experimentally tested. First, the same type of speckle pattern represented in figure 1 was attached precisely to the surface of a planar target. Then an LSD shaker was used to vertically vibrate the target in different frequencies and amplitudes. The frequency of motion was increased from 5 to 10, 15 and 20 Hz and the amplitude of shaker was changed from 0.5 mm (1.5px) to 1.5mm (4.5px), 3mm (9px), 5mm (15px) and 7mm (21px). Target's motion was recorded by a digital camera with frame rate of 11, 16, 20 or 21 depending on the specific test (due to the limited frame rate of the used camera (25 fps at full resolution), the tests were done in controlled aliasing condition). The object's position was simultaneously measured with a high resolution laser interferometer. The specifications of the experimental setup are reported in Table 2.

Table 2. Experimental set up.

	Device	Brand and Type	Specifications
1	Shaker	LSD, V830-335 TRUNNION	Max Frequency = 3 kHz Max Mass = 12kg Max Sinusoidal Speed = 2.0 m/s
2	Camera	AVT Marlin F131B	Equipped with a 280x1024 CMOS sensor Lens' s Nominal Focal Length = 16mm
3	Laser Interferometer	PSV300	Single point Polytec Scanning Vibrometer Resolution = 2.56μm

Part of the images taken by the camera during one cycle of the motion (starting and ending in static position), are demonstrated in Figure 16. The speckle pattern was square shaped with size of 100mm (300 pixels) and average grain size of 4 pixels. The motion effect is more visible in neutral position where the velocity is maximum (Figure 16).

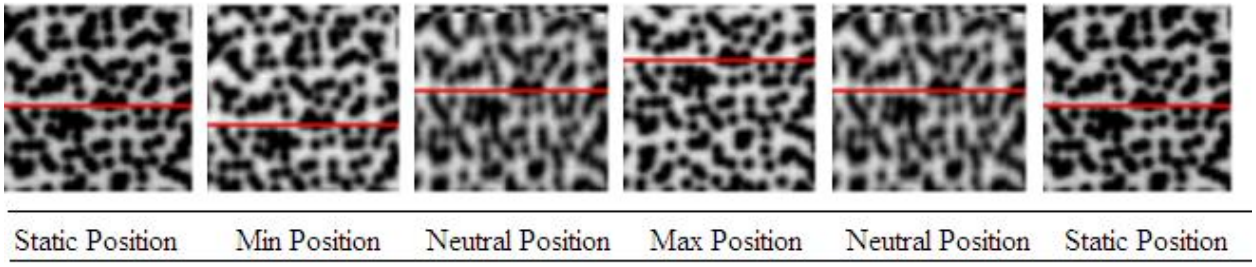

Figure 16. A part of a typical image taken by the camera in one cycle of the motion starting and ending in static position. The red horizontal line is sketched to give better understanding of the sinusoidal vibration.

In this case, DIC estimated displacements were compared with the corresponding values measured by the laser interferometer. The result is reported in terms of discrepancy which has been defined as the absolute difference between time histories of estimated displacement (by DIC) and reference displacement (measured by laser interferometer) (Figure17). The mean of discrepancy was negligible in respect to the standard deviation; therefore the standard deviation of discrepancy is reported here.

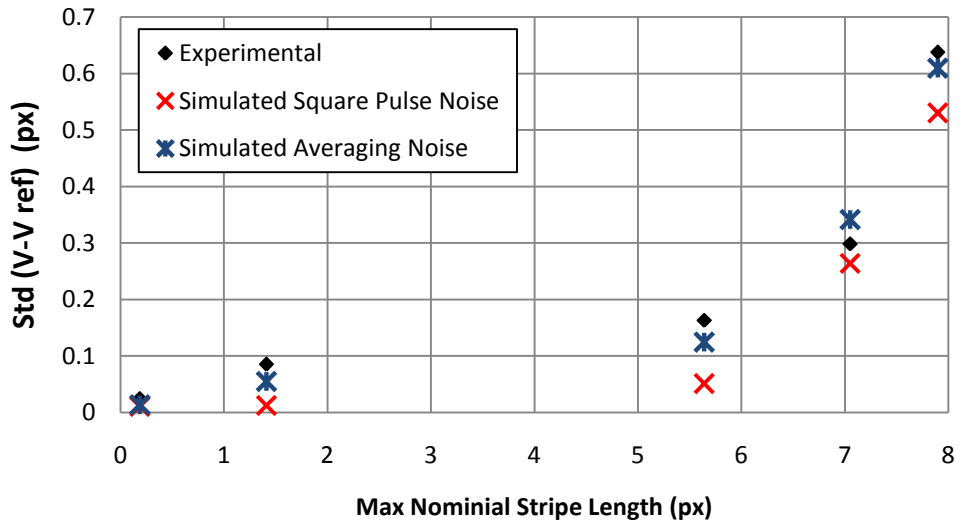

Figure 17. Simulation of few sinusoidal vibration tests and the corresponding experimental validation. The vertical axis is the standard deviation of discrepancy.

Figure 17 shows a good agreement between the simulations and the experiments. As we expected before the averaging method, simulates better the reality in this motion condition.

CHAPTER 5

Experimental Uncertainty Assessment of DIC

Several harmonic motion tests were conducted in order to experimentally asses the uncertainty of DIC. The result can be divided into two man sections: Displacement estimation (section 5.1) and strain estimation (section 5.2).

5.1 Displacement Estimation

In this section, DIC technique is implemented in order to estimate not the instantaneous position of the target but the amplitude of the sinusoidal vibration. The results again are reported in terms of the standard deviation of discrepancy reminding that the mean of discrepancy was negligible compared to the corresponding standard deviation.

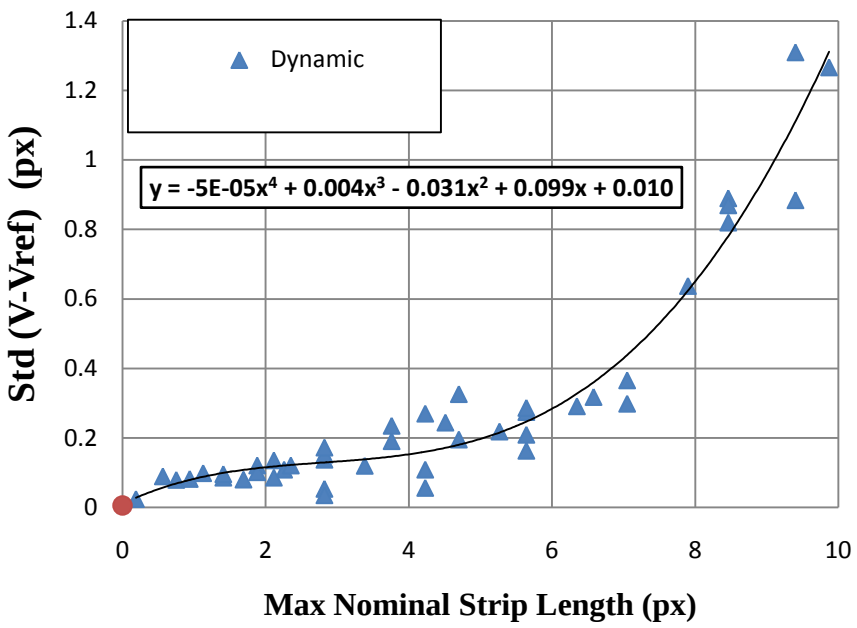

Figure 18. Standard Deviation of Discrepancy with respect to Max nominal stripe length in real tests.

Figure 18, represents a quadratic polynomial fit for the test results. The value of vertical axis offset is equivalent to the DIC displacement uncertainty in static condition. This value has been reported in [43], to be equal to 0.006 px (circular market). This graph proves that, our estimated trend is in a great agreement also with the results of that study.

In Figure 19, the same results as Figure 18 are plotted but this time with respect to the ratio of exposure time to period of the harmonic motion named as E2PR. It is a relevant parameter in the case of vibration motion.

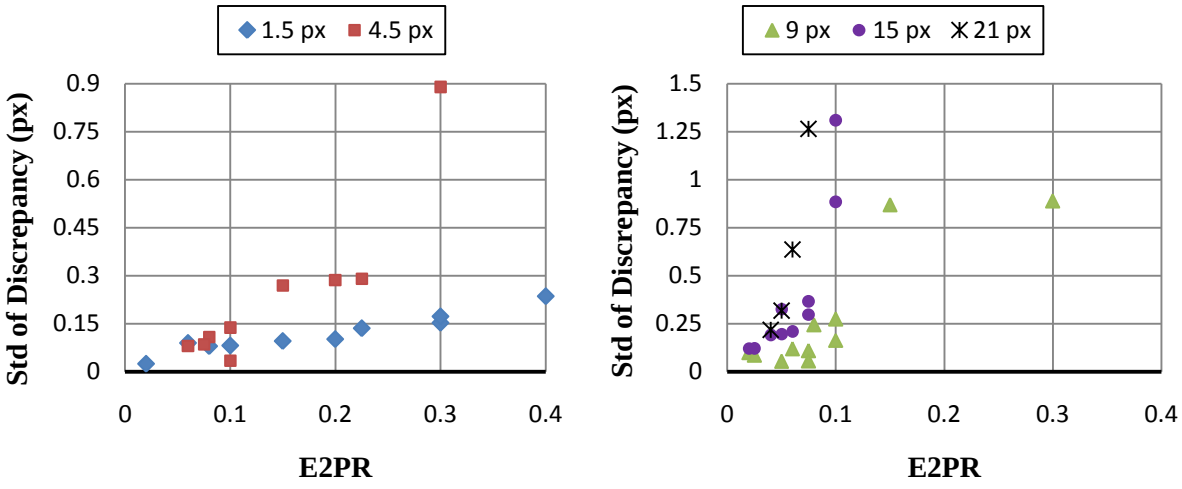

Figure 19. Experimental standard deviation of discrepancy in case of Displacement estimation in respect to E2PR for different Amplitude values [Amplitude = 1.5px, 4.5px (left) and Amplitude=9px, 15px, 21px (right)].

Standard deviation of discrepancy increases exponentially with the E2PR and the larger is the amplitude of motion the larger is the growth rate (Figure19).

5.2 Strain Estimation

The target dose not deform during the tests therefore, the corresponding value of strain is expected to be zero. On the other hand, while using the DIC technique a small out of plain motion could be mistakenly interpreted as strain. Figure 20 represent mean and standard deviation of the strain estimated by DIC in respect to Max nominal stripe length.

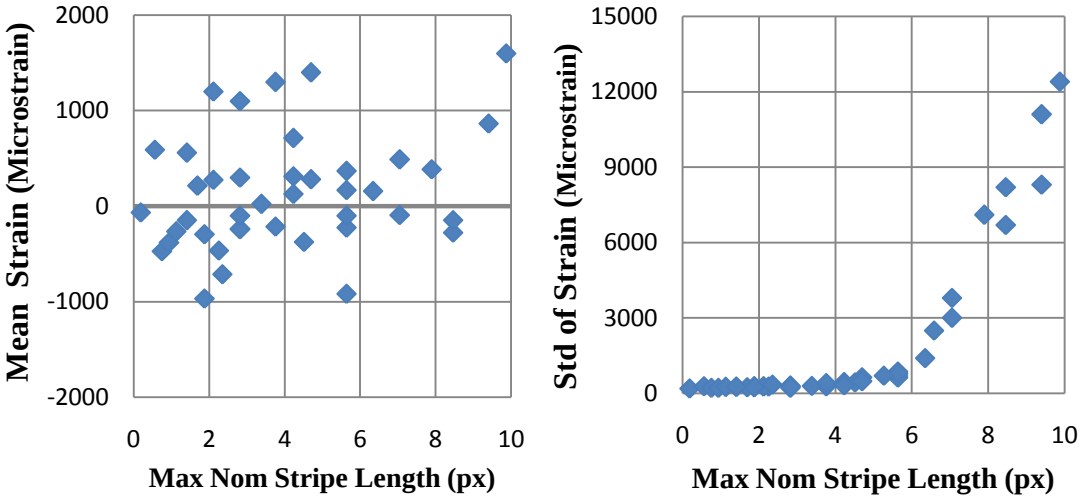

Figure 20. Experimental Strain mean and standard deviation estimated by DIC in respect to Max nominal stripe length.

Strain mean is randomly distributed around zero while the standard deviation shows an increasing trend. This growth rate is much faster when the strip length surpasses 6 pixels (Figure 20).

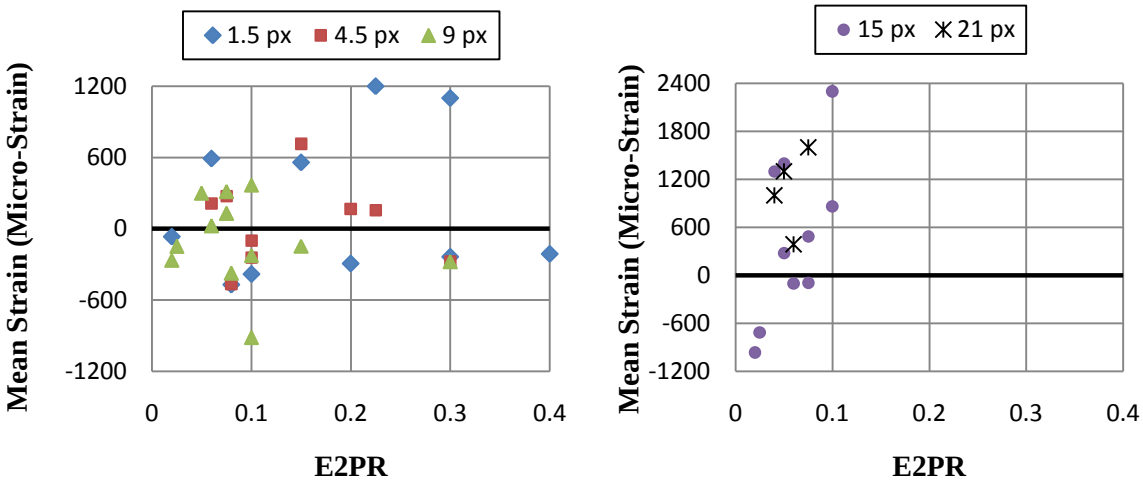

Figure 21. Experimental strain mean estimated by DIC in respect to E2PR for different Amplitude values [Amplitude = 1.5px, 4.5px, 9px (left) and Amplitude=15px, 21px (right)].

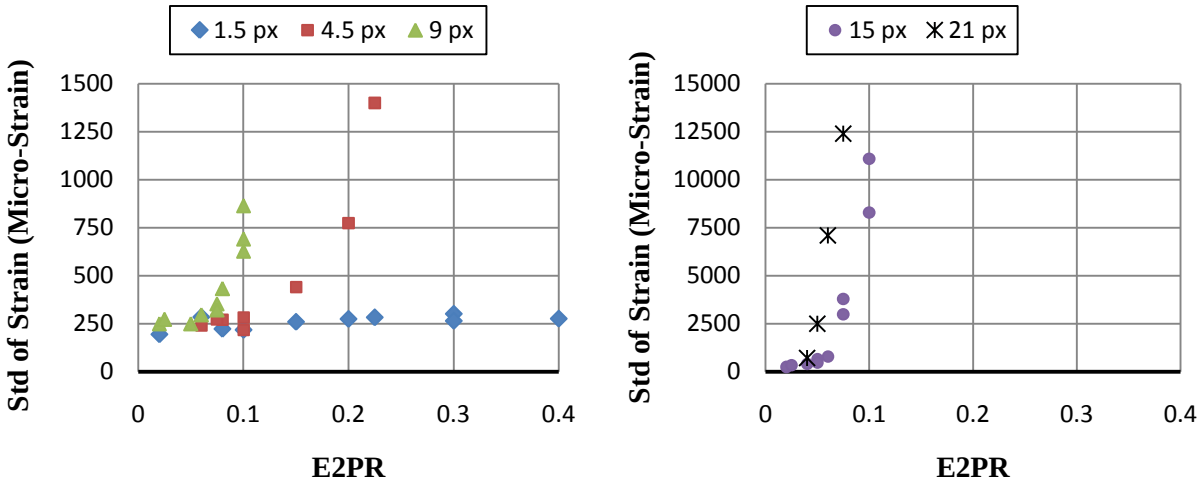

Figure 22. Experimental strain standard deviation estimated by DIC in respect to E2PR for different Amplitude values [Amplitude = 1.5px, 4.5px, 9px (left) and Amplitude=15px, 21px (right)].

Mean estimated strain does not show a specific dependence on E2PR while the corresponding standard deviation increases exponentially with the E2PR. The larger is the amplitude of motion, the larger is the growth rate (Figure 21 and Figure 22).

As it was mentioned earlier, presence of motion effect in the acquired images is an important source of DIC uncertainty. Moreover, analyzing experimental vibration tests proves that if the motion effect value w (strip length) surpasses a critical limit, the DIC technique will no longer be able to correlate. Therefore it can be claimed that the presence of motion effect defines a limit for implementation of DIC in dynamic conditions. Based on the analysis of more than 70 cases, this critical motion effect value is about 8 pixels.

CHAPTER 6

Deconvolution Analysis and DIC Uncertainty Improvement

In the previous chapters, the motion effect, present in dynamic acquisitions was simulated by convolving the reference image with the proper square pulse function. In the current chapter we perform a deconvolution analysis aiming to estimate the motion effect present in an acquired image. This type of analysis can be done by determining the specific square pulse which could be convolved with the reference image (static image) to recreate the acquired image with motion effect. Once the square pulse is determined, the corresponding width would be an estimation of motion effect and the shift would represent the net displacement.

Deconvolution analysis could be a helpful procedure when implementing DIC in dynamic applications. It allows estimating the value of motion effect w within each image and since the motion effect w has a known influence on the uncertainty of measurement (see Chapter 3 and Chapter 4); this type of analysis could be a reliable technique to estimate the uncertainty in the displacement estimation. Deconvolution can also be used to improve the uncertainty of DIC in dynamics. As it was previously pointed out an important source of DIC uncertainty in dynamic applications is the motion effect, present in the acquired image. This motion effect could be known thanks to the deconvolution analysis and can be added to the reference image by using the technique discussed in section 3.3.3, in order to generate a new image. This image would be the reference image with added motion effect the same as the one present in the acquired image. Now if we consider this generated image as the new reference image we expect to be able to decrease the contribution of motion effect (i.e. blurring) in the final uncertainty of displacement estimation.

The current chapter addresses two main issues. First in section 6.1, deconvolution technique is implemented to estimate the motion effect within a given image. As the next

step, this technique will be used to improve DIC uncertainty in dynamic conditions (section 6.2).

6.1 Deconvolution for Motion Effect Estimation

Deconvolution technique could be performed through few simple steps:

1) First of all, the Discrete Fourier Transform (DFT) of a row (in the case of horizontal motion) or a column (in the case of vertical motion) should be calculated.
2) The ratio of the obtained matrix to the DFT of the same row number (or column number) in the reference image needs to be found.
3) Repeat this procedure for all the rows (or columns) and average these results. Keep in mind that, this ratio signal is in frequency domain. (This ratio is supposed to be equivalent with the DFT of the desired square pulse. The square pulse will be determined in the next two steps).
4) Considering the fact that the Fourier transform of a square pulse is a sinc function, determining the desired square pulse would be easier in frequency domain. Therefore The fourth step would be finding a sinc function in frequency domain which matches the best, the obtained ratio signal.
5) Once the sinc function is known, the parameters of the corresponding square pulse (width and offset) can be easily determined.

The deconvolution technique will be implemented in two different cases: Numerically generated images section (6.1.1) and experimentally acquired images (6.2.1).

6.1.1 Estimating Motion Effect in Numerically Generated Images

As the first step to evaluate the performance of this technique for motion effect estimation, a set of shifted images with motion effect were generated using the method discussed in section [3.3.3]. This could be a trustable approach to check the reliability of the deconvolution analysis outcome, since the motion effect w of each image is already known. Figure 23, shows the bias error in estimation of motion effect and the corresponding shift in a specific case. The image set is generated by imposing simultaneously motion effect and shift to the filtered reference image (Figure 1). The

value of motion effect varies from zero to 8 px with step of 0.1px (w=0:0.1:8) and the shift in each image is chosen to be twice the corresponding w (shift=2w, as an example. The image with motion effect w=2px has imposed shift=4px).

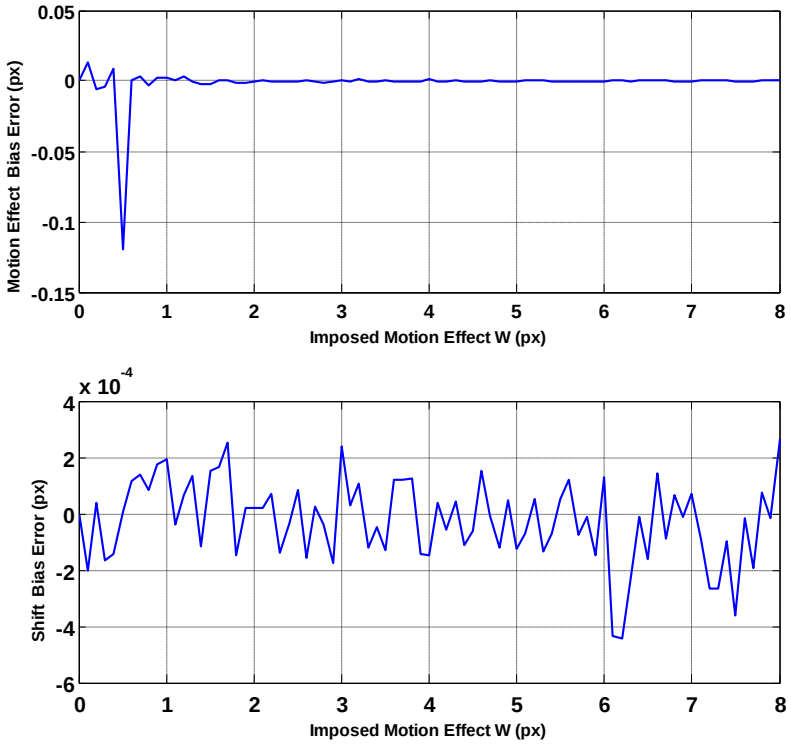

Figure 23. Bias error in estimation of motion effect and shift in the case of generated images. The image set imposing a motion effect that varies from zero to 8 px with step of 0.1px (w=0:0.1:8) and a shift in each image that is chosen to be twice the corresponding w (shift=2w).

According to Figure 23, deconvolution analysis is able to estimate the motion effect in the case of numerically generated images with bias error less than 0.12 pixels. This technique works much better when the motion effect is larger than w=1. The reason can be explained by considering Figure 24 and Figure 25. In these two figures the ratio signal and the corresponding fitted sinc function are plotted for two levels of motion effect values (w=0.5 px and w=7.5 px). The graphs show better fitting when it comes to higher motion effect values (Figure 25), while in the lower motion effect cases in which the amplitude of the ratio signal is almost constant (close to one), the fluctuations in the curve can be critical and misleading for fitting the sinc function (Figure 24). This can explain the presence of the initial peek in the motion effect bias error curve (Figure 23).

Even though the presence of the peek in motion effect bias error curve demonstrates that this technique is not as accurate in the case of smaller w values, the accuracy is still acceptable for the purpose of this work. This statement can be explained by reminding the fact that the influence of motion effect on uncertainty of DIC is almost negligible when w is smaller than one pixel (Figure 8). The real concern while implementing DIC is when the motion effect on the acquired images is significant (larger w values). It can be also noticed that the deconvolution analysis is even more accurate in estimation of shift than the motion effect (Figure 23).

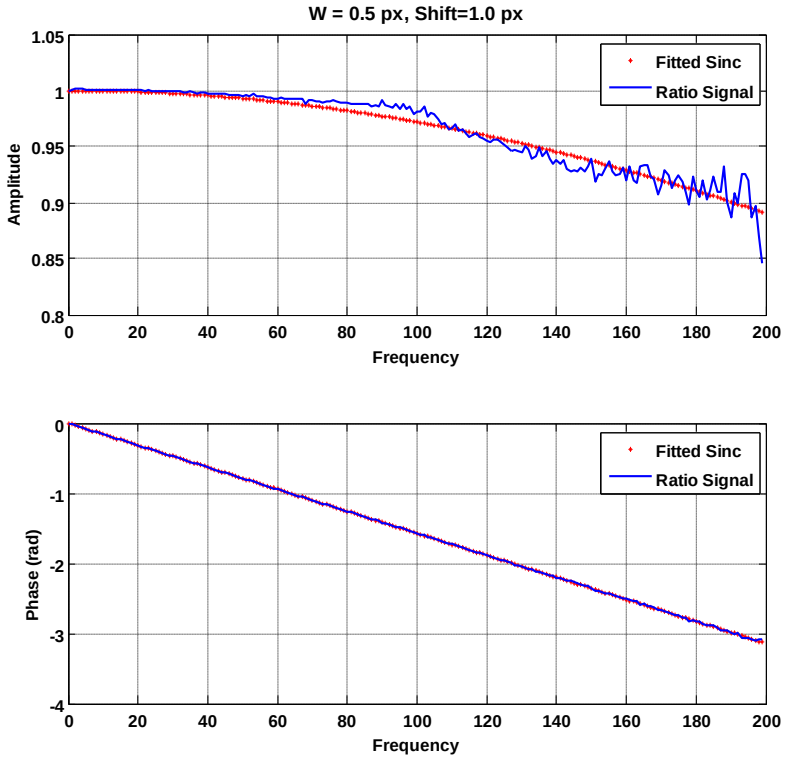

Figure 24. Ratio signal and the corresponding fitted sinc function in frequency domain after performing the deconvolution analysis on a generated image with imposed motion effect w=0.5 px and shift=1.0 px. The horizontal axis is frequency that varies from zero to Nyquist frequency.

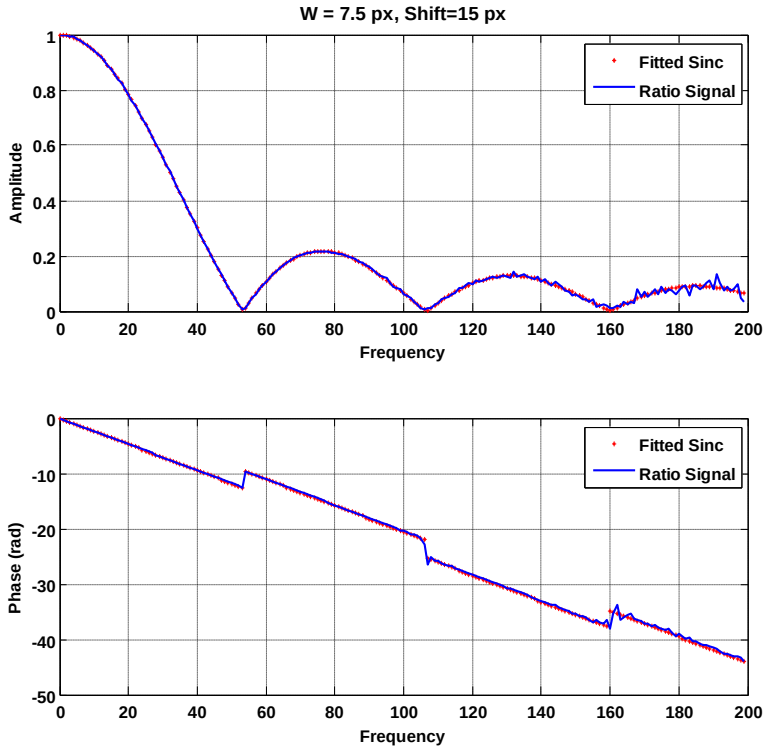

Figure 25. Ratio signal and the corresponding fitted sinc function in frequency domain after performing the deconvolution analysis on a generated image with imposed motion effect w=7.5 px and shift=15 px. The horizontal axis is frequency that varies from zero to Nyquist frequency.

6.1.2 Estimating Motion Effect in Experimentally Acquired Images

Although the performance of Deconvolution technique is proven to be acceptable in the case of numerically generated images (see section 6.1.1), the important issue is how it performs on the images acquired in a real dynamic test. In order to answer this question the same analysis has been carried out in the cases of two sinusoidal vibration tests. Therefore, for every frame of each test, the deconvolution technique has been implemented and the estimated motion effect w and the corresponding shift were obtained. Case 1 is a sinusoidal vibration test with higher E2PR, while Case 2 has the lower E2PR. Considering these two cases allows us to check if the performance of the deconvolution method depends on E2PR.

6.1.2.1 Case 1, higher E2PR

Table below represents the specifications of Case 1.

Table 3. Specifications of the real test, Case 1.

Test Data (Case 1)	
Frequency (Hz)	15
Amplitude (px)	4.5
Exposure Time (ms)	15
$\frac{\text{Eposure time(s)}}{\text{Period(s)}}$	0.225
Max Nominal Stripe Length (px)	6.35
Frame Rate (Frame/s)	16

In Figure 26, the ratio signal and the corresponding fitted sinc function is plotted for seventh frame of the experiment (this frame corresponds to the highest motion effect value). It is better to consider only the low frequency data (first lobe) for fitting the sinc function because there is much better matching between the two curves in this frequency range. In this way the estimation of w could be improved.

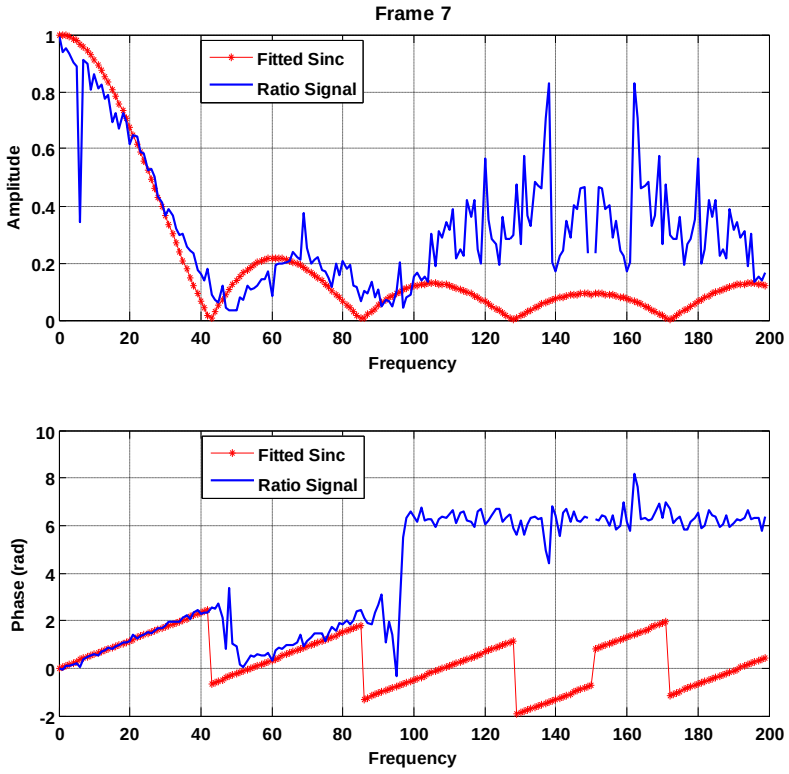

Figure 26. Ratio signal and the corresponding fitted sinc function in frequency domain after performing the deconvolution analysis on a seventh frame of the real test. The horizontal axis is frequency that varies from zero to Nyquist frequency (Case 1).

The same procedure has been done for every frame and the estimated motion effect and shift is reported in Table4 and Figure 27. Motion effect value is the largest in frame 7 and 15 because they correspond to the time when the velocity of the target is the highest (zero crossing points in the sinusoidal motion).

Table 4. Estimated w in each frame of real test obtained by deconvolution (Case 1).

Frame	1	2	3	4	5	6	7	8	9	10	11	12	13	14	15	16	17
Estimated w (px)	5.9	3.8	1.8	2.4	4.6	6.3	6.9	6.3	4.5	2.4	0	1.6	3.1	5.0	6.9	6.8	5.9

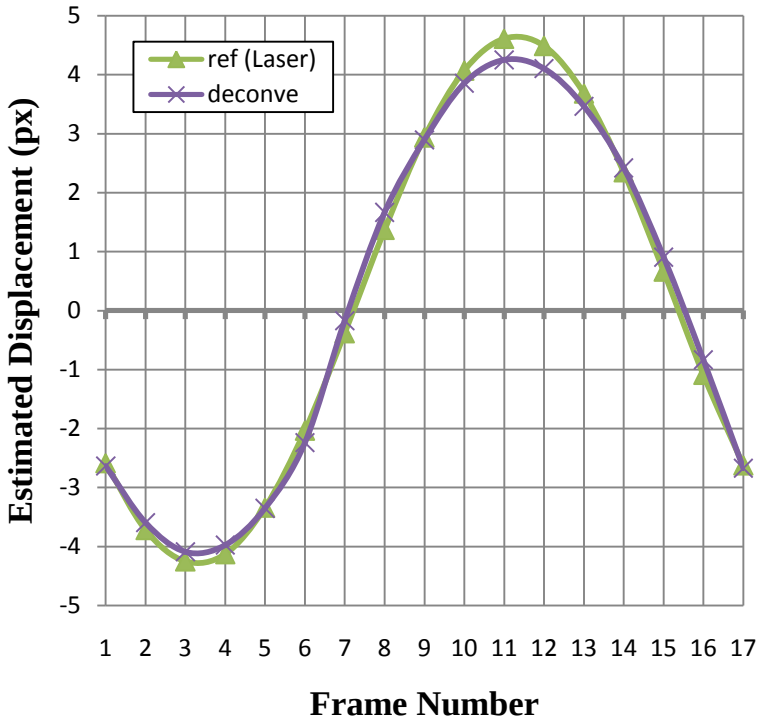

Figure 27. Estimation of Displacement Using Deconvolution technique (Case 1).

Figure 27, represents a better estimation of the displacement in the frames close to the neutral position while the deconvolution technique underestimates the peek.

6.1.2.2 Case 2, Lower E2PR

Table below represents the specifications of Case 2.

Table 5. Specifications of the real test, Case 2.

Test Data (Case 2)	
Frequency (Hz)	15
Amplitude (px)	21 px (7 mm)
Exposure Time (ms)	5
E2PR	0.075
Max Nominal Stripe Length	9.8729 Pixels
Frame rate	16

In Figure 28, the ratio signal and the corresponding fitted sinc function is plotted for the first frame of the experiment (this frame corresponds to the zero crossing). Only the first lobe of the ratio signal was used for fitting the sinc function. The reason is already discussed in the section 6.1.2.1. The same procedure has been done for every frame of the test and the estimated motion effect is reported in Table6.

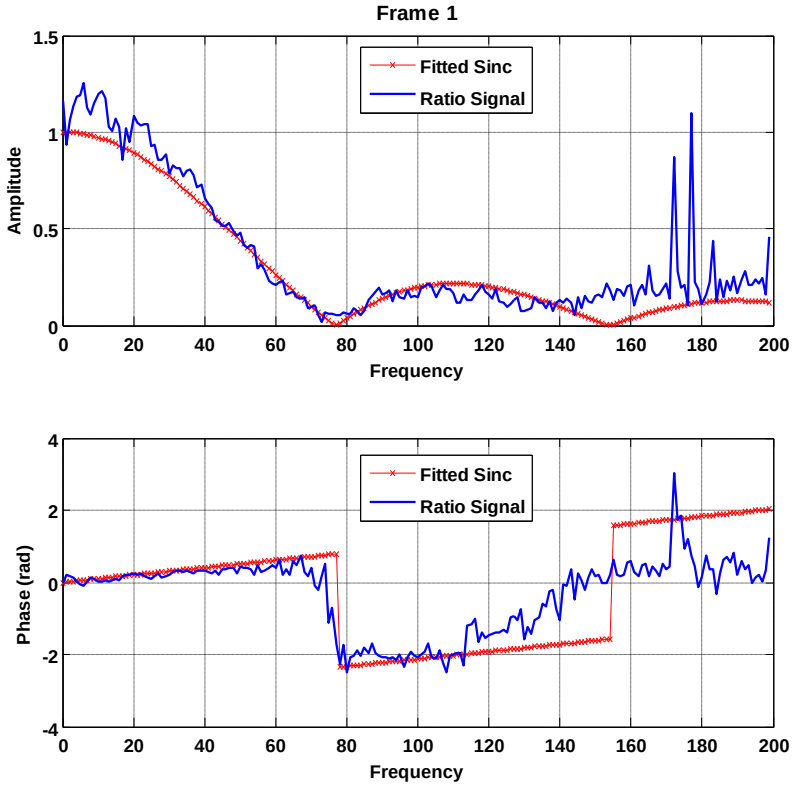

Figure 28. Ratio signal and the corresponding fitted sinc function in frequency domain after performing the deconvolution analysis on a seventh frame of the real test. The horizontal axis is frequency that varies from zero to Nyquist frequency (Case 2).

The laser position data allows calculating displacement of the target during the exposure time in each frame of the motion. This displacement value is equivalent to the reference w in that particular frame (Table 6, second row). Motion effect value is the largest in frame 1, 9 and 17 because they correspond to those moments in which the velocity of the target is the largest (zero crossing points in the sinusoidal motion).

Table 6. Estimated w in each frame of real test obtained by deconvolution and the corresponding reference value (Case 2).

Number	1	2	3	4	5	6	7	8	9	10	11	12	13	14	15	16	17
Estimated w (px)	9.7	9.4	7.3	4.1	1.1	4.1	7.1	8.7	9.2	9.0	6.8	4.2	1.3	3.5	6.5	8.9	9.6
Ref w (px)	9.9	9.4	7.4	3.9	0.6	3.9	7.0	8.9	9.5	8.7	6.8	3.9	0.8	3.2	6.4	8.8	9.9

Figure 29, represents the bias error in estimation of motion effect w using the deconvolution technique. According to Figure 29, the bias error does not exceed 0.6 in one cycle of the motion and therefore the accuracy of this technique is in an acceptable range for the purpose of this work (see section 6.1.1).

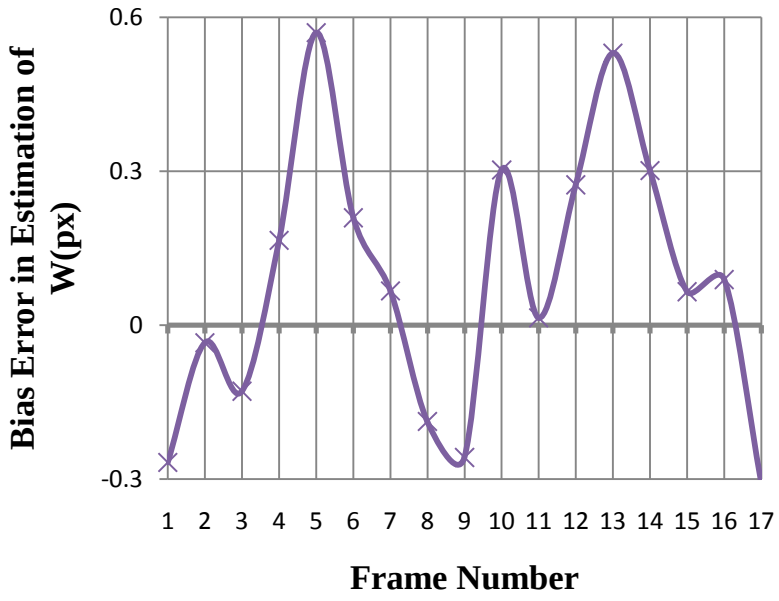

Figure 29. Bias Error in Estimation of motion effect W (px), using Deconvolution technique (Case 2).

The deconvolution technique was also used to estimate the displacement of the motion. Figure 30 compares this result with the laser data.

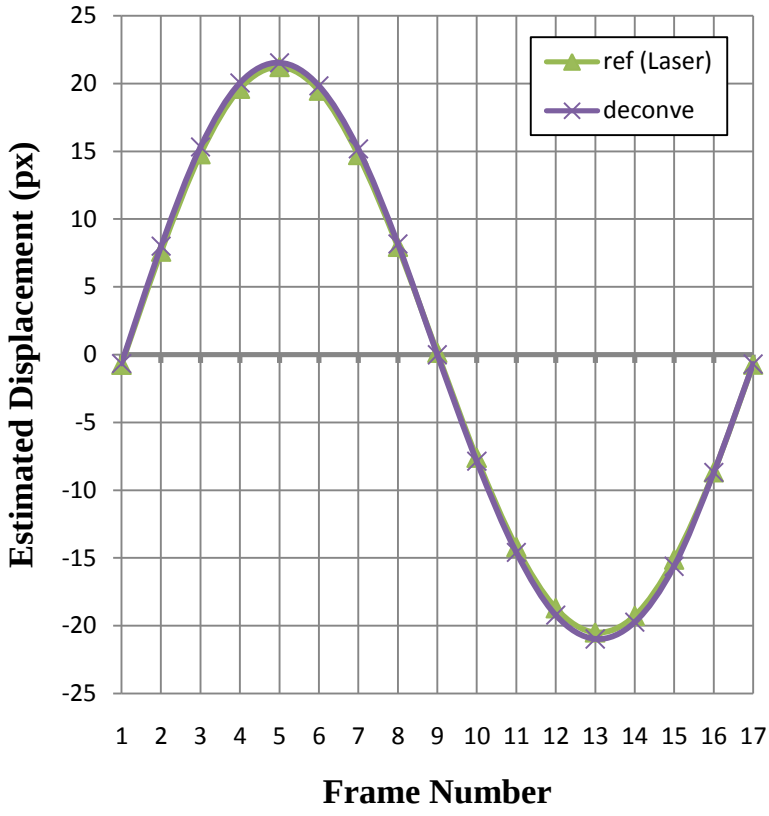

Figure 30. Estimation of Displacement Using Deconvolution technique (Case 2).

Comparing the results obtained in Figure 27 and Figure 30 is important. As it can be seen in Case 2 in which we are dealing with lower E2PR, underestimation of the peek is less visible while in the case of higher E2PR (Case 1) this underestimation is not negligible. Figure 31, helps to explain the issue of peek underestimation. The red line represents the motion of the target during the exposure time. Using the deconvolution technique does not allow us to find the position of the maximum but instead determines an intermediate position. Therefore as the value of exposure time (and therefore E2PR) increases the strip length covered by the target grows and as a result the underestimation increases as well. Based on this explanation, it be claimed that the underestimation of the peek is not due to image processing technique but it is due to the motion effect.

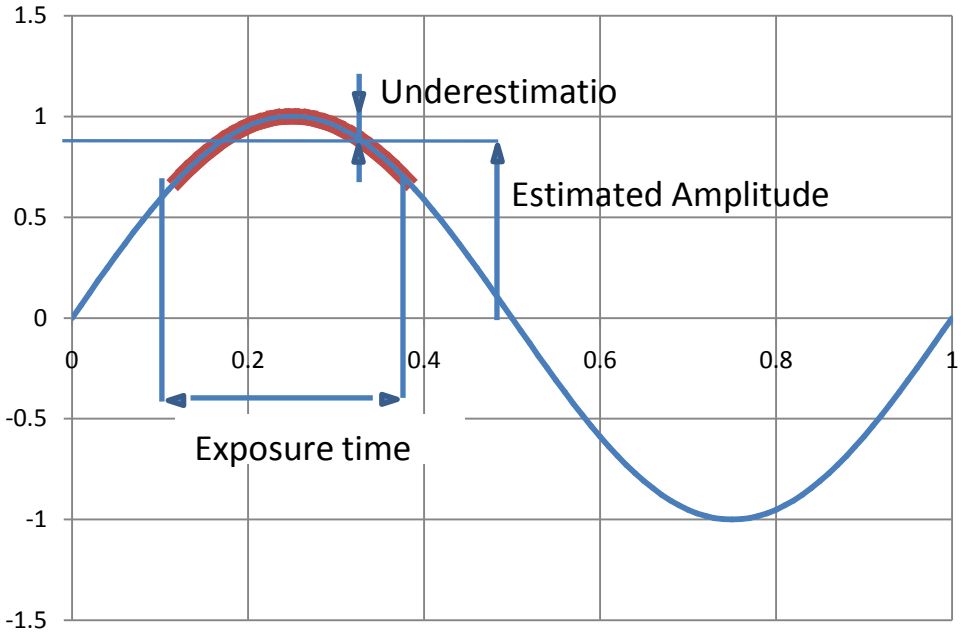

Figure 31. Peek underestimation due to motion effect.

It should be also mentioned that in theory, the deconvolution approach estimates the displacement reliably as long as we are dealing with rigid motion and constant lighting.

6.2 Deconvlotion for Improving DIC Uncertainty in Dynamics

As it was mentioned briefly earlier, Deconvolution can also be used to improve the uncertainty of DIC in dynamics. The idea is to generate a new reference image that has the same motion effect as the one acquired in a dynamic condition. Therefore the steps below need to be done:

1) Perform the deconvolution analysis on an acquired image in order to determine the motion effect value w. (see section 6.1)

2) Using the technique discussed in section [3.3.3], we are able to analytically convolve the reference image with a zero centered square pulse which has a width equal to w estimated by deconvolution (step one). This new image can be considered as the new reference image.

This technique has been implemented in both cases of the sinusoidal vibration tests (Table 3 and Table 5).

6.2.1 Case 1, Higher E2PR

From the deconvolution analysis the motion effect w is already known for every frame (Table 4). As the next step, this estimated w has been used to generate the new reference image for each frame. Then, the DIC analysis has been carried out. Figure 32 and Figure 33, compares the results of the improvement technique with that of the normal DIC. They demonstrate that this technique is able to significantly improve the displacement estimation and the corresponding standard deviation graph. Studying the discrepancy of the result related to Case 1, reveals that with the help of deconvolution, the matching between DIC and laser Interferometer measurement improves by 31%. Figure 32 proves that the issue of peek underestimation does still exist even in the case of DIC. (See section 6.1.2.2)

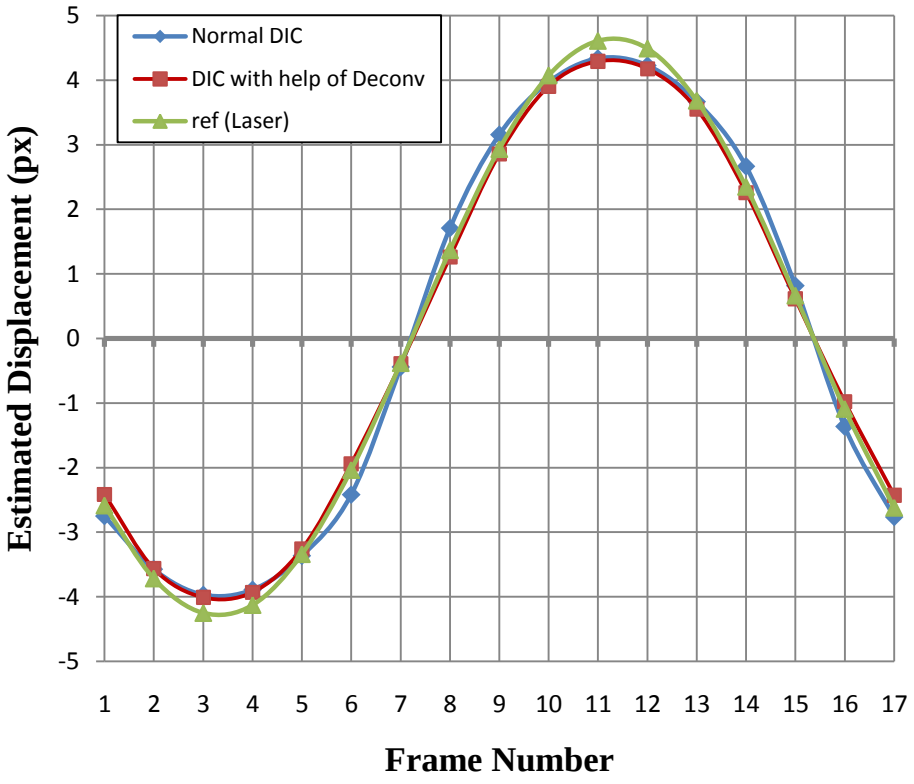

Figure 32. Estimated displacement in every frame of the real test (Case 1).

As it was mentioned earlier, frames acquired when the target is passing the neutral position are the ones with the largest values of motion effect. That is why the normal DIC technique estimates the displacement with higher uncertainty values in zero crossing frames. This can explain the presence of the peeks in Figure 33, which correspond to frame 7 and 15.

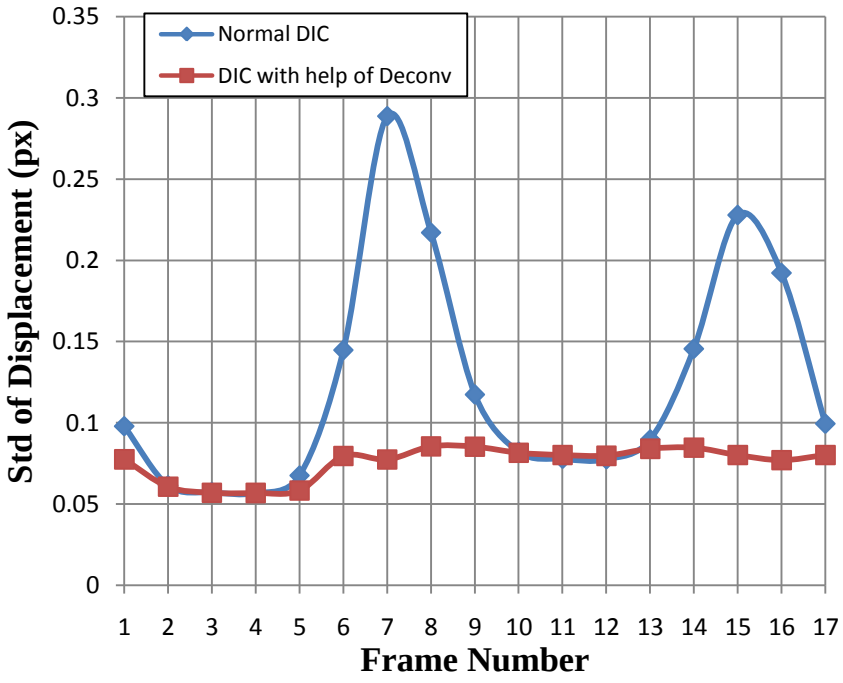

Figure 33. Standard deviation of estimated displacement in every frame of the real test (Case 1).

6.2.2 Case 2, Lower E2PR

From the deconvolution analysis the motion effect w is already known for every frame (Table 4). As the next step, this estimated w has been used to generate the new reference image for each frame. Then, the DIC analysis has been carried out. Figure 34 and Figure 35, compares the results of the improvement technique with that of the normal DIC. They demonstrate that this technique is able to significantly improve the displacement estimation and the corresponding standard deviation graph. Studying the discrepancy of the result related to Case 2, reveals that with the help of deconvolution, the matching between DIC and laser Interferometer measurement improves by 71%.

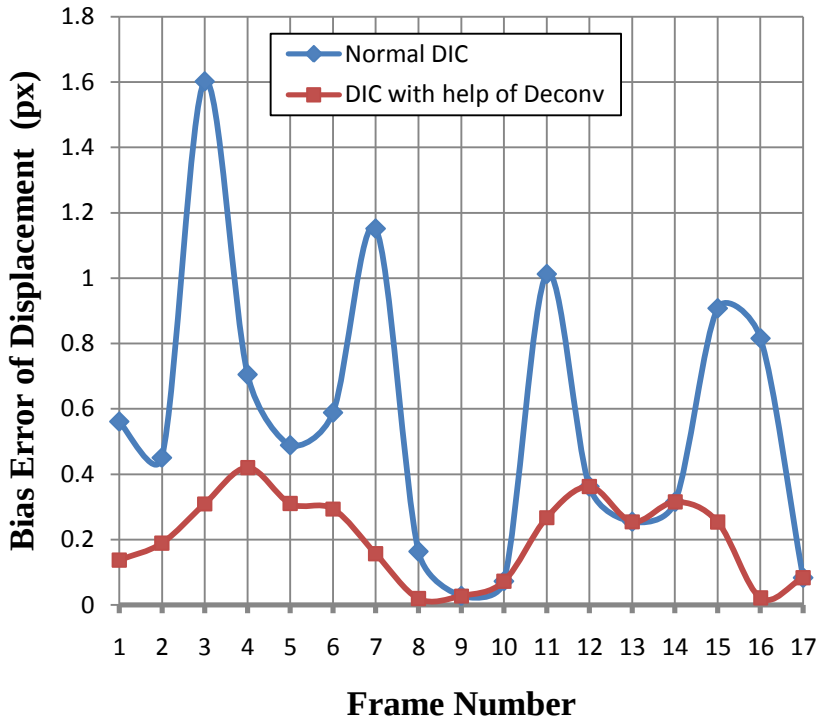

Figure 34. Estimated displacement in every frame of the real test (Case 2).

As it was mentioned earlier, frames acquired when the target is passing the neutral position are the ones with the largest values of motion effect. That is why in Figure 35 the normal DIC technique estimates the displacement with higher uncertainty values in zero crossing frames.

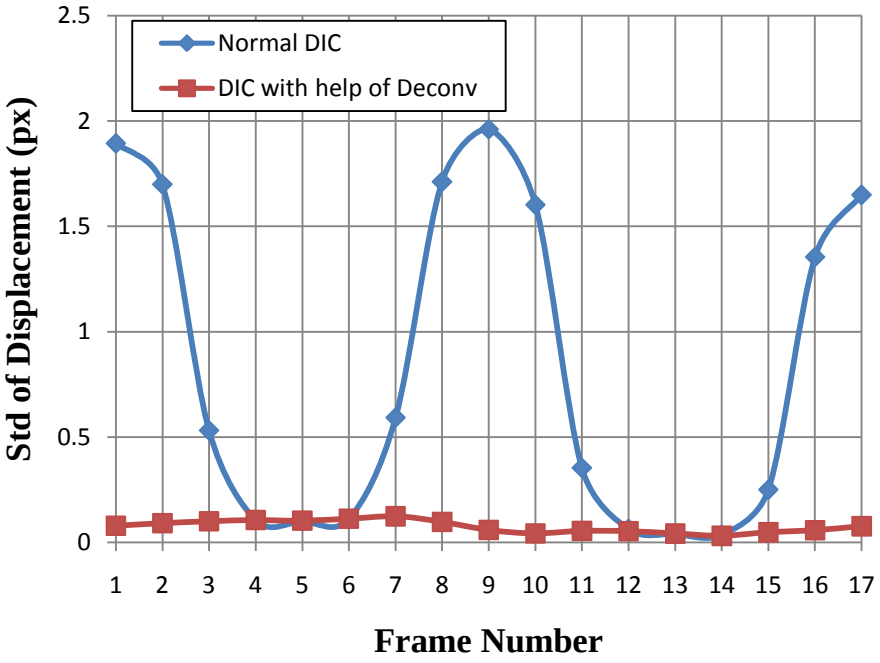

Figure 35. Standard deviation of estimated displacement in every frame of the real test (Case 2).

CHAPTER 7

Conclusion

In dynamics, dealing with a moving target, causes a motion effect (i.e. blurring) on the acquired images. This factor is an important source of measuring uncertainty while implementing Digital Image Correlation (DIC) technique. In the present study, DIC's uncertainty in dynamic conditions was evaluated and improved.

The whole work can be divided in to two main parts. In the first part, two different methods to simulate the motion effect on a reference image were proposed, discussed and validated. These methods allow simulating the acquired images in a real dynamic test and estimating the measurement uncertainty caused by the motion effect. The validation of the simulation was performed by experimentally creating the simulated cases. Therefore, the corresponding harmonic motion was imposed to an object, while it was captured by a camera and it's position was measured by a laser interferometer. The results show good agreement between the experiments and the simulations. Providing known testing condition (in particular the relation between target velocity and camera shutter time), the presented method can consequently be exploited to quantify the motion induced uncertainty in dynamic DIC measurements simply starting from a reference unblurred image of the measurement surface.

After conducting further sinusoidal vibration tests, the DIC uncertainty in estimation of the displacement and strain was also experimentally assessed. Both the strip length and the ratio of exposure time to harmonic motion period (named as E2PR) are demonstrated to be relevant parameters which influence the measurement uncertainty trends.

In the second part of the study a numerical technique was proposed to estimate the motion effect present in an acquired image. This technique gives two main advantages. First, since the motion effect itself has a known influence on the uncertainty of measurement (thanks to the first part of the study), we will be able to predict the DIC's uncertainty by just having an acquired image. Second, this numerical technique was used

to improve the uncertainty of DIC in dynamic applications. In this way the bias error and the uncertainty of the measurements were considerably decreased.

7.1 Future work

This study focused on 2D DIC. In the case of 3D DIC similar problems are expected to arise and therefore, a complete understanding of two dimensional conditions will be of great help to further studies which deal with 3D conditions. As the future work all the theoretical and experimental approaches could be extended to 3D applications.

References

[1] M. Bornert, F. Br émand, P. Doumalin, J.C. Dupr´e, M. Fazzini, M. Gr´ediac, F. Hild, S. Mistou, J. Molimard, J.J. Orteu, L. Robert, Y. Surrel, P. Vacher, B. Wattrisse, Assessment of digital image correlation measurement errors: methodology and results, Experimental Mechanics 49 no.3 (2009) 353-370.

[2] T. Schmidt, J. Tyson, K. Galanulis, Full-field dynamic displacement and strain measurement using advanced 3D image correlation photogrammetry, Experimental Techniques, 27(3) (2003) 47-50.

[3] Wang, Xiaoyan, Tang Yi, Qiuyan Tang, Liang Feng, Guoqiang Ni, Liwei Zhou, Simulation and analysis of vibration blurred images, Wireless Communications Networking and Mobile Computing (WiCOM) IEEE (2010) 1-4.

[4] Hubert, W. Schreier, M. A. Sutton, Systematic errors in digital image correlation Due to undermatched subset shape functions, Experimental Mechanics, 42(3) (2002) 303-310.

[5] T. Siebert, T. Becker, K. Spiltthof, I. Neumann, R Krupka, High-speed digital image correlation: error estimations and applications**,** Optical Engineering 46(5) May 2007 051004.

[6] V. Tiwari, M.A. Sutton, S.R. McNeill, Assessment of high speed imaging systems for 2D and 3D deformation measurements: Methodology development and validation, Experimental Mechanics 47 (2007) 561–579.

[7] G.J. Um, H.J. Kim, Experimental error assessment for image correlation analysis on a paper tensile specimen, J. Ind. Eng. Chem. 13(2) (2007) 214-218.

[8] H. Haddadi, S. Belhabib, Use of rigid-body motion for the investigation and estimation of the measurement errors related to digital image correlation technique, Optics and Lasers in Engineering 46 (2008) 185–196.

[9] B. Pan, K. Qianb, H. Xiec, A. Asundia, On errors of digital image correlation due to speckle patterns, ICEM 7375 (2008) z1:z7.

[10] J. M. Vassolera, E. A. Fancelloa, Error analysis of the digital image correlation method, Mecánica Computacional 24, (2010) 6149-6161.

[11] M. Fazzini, S.Mistou, O.Dalverny, L.Robert, Study of image characteristics on digital image correlation error assessment, Optics and Lasers in Engineering 48 (2010) 335–339.

[12] Z. Hu, H. Xie, J. Lu, H. Wang, J. Zhu, Error evaluation technique for three-dimensional digital image correlation, Applied Optics 50(33) Nov (2011) 6239-6247.

[13] H.W. Schreier, J.R. Braasch, M.A. Sutton, Systematic errors in digital image correlation caused by intensity interpolation, Opt. Eng. 39(11) (2000) 2915-2921.

[14] Z.Y. Wang, H.Q. Li, J.W. Tong, J.T. Ruan, Statistical analysis of the effect of intensity pattern noise on the displacement measurement precision of digital image correlation using self-correlated images, Experimental Mechanics 47 (2007) 701–707.

[15] P.L. Reu, M. Sutton, Y. Wang, T.J. Miller, Uncertainty quantification for digital image correlation, Proceedings of the SEM Annual Conference June (2009) Albuquerque New Mexico USA.

[16] Y.Q. Wang, M.A. Sutton, P.L. Reu and T.J. Miller, Image matching error assessment in digital image correlation, Proceedings of the SEM Annual Conference June (2009) Albuquerque New Mexico USA.

[17] Y. Q. Wang, M. A. Sutton, H. A. Bruck and H. W. Schreier, Quantitative error assessment in pattern matching: Effects of intensity pattern noise, interpolation, strain and image contrast on motion measurements, Strain 45 (2009) 160–178.

[18] Y.Q. Wang, M.A. Sutton, X.D. Ke, H.W. Schreier, P.L. Reu, T.J. Miller, On error assessment in stereo-based deformation measurements Part I: Theoretical developments for quantitative estimates, Experimental Mechanics 51 (2011) 405–422.

[19] X.-D. Ke, H.W. Schreier, M.A. Sutton, Y.Q. Wang, Error Assessment in Stereo-based Deformation Measurements Part II: Experimental Validation of Uncertainty and Bias Estimates, Experimental Mechanics 51 (2011) 423–441.

[20] T. Schmidt, J. Tyson, and K. Galanulis, Full-field dynamic displacement and strain measurement-specific examples using advanced 3D image correlation photogrametery: part1, Experimental Techniques May/June (2003) 47-50.

[21] T. Schmidt, J. Tyson, K. Galanulis, Full-field dynamic displacement and strain measurement—specific examples using advanced 3D image correlation photogrametery: part2, Experimental Techniques, July/August (2003) 22-26.

[22] M.S. Kirugulige, H.V. Tippur, T.S. Denney, Measurement of transient deformations using digital image correlation method and high-speed photography: application to dynamic fracture, Applied Optics 46(22) August (2007) 5083-5096.

[23] W. Wang, J.E Mottershead, C. Mares, Vibration mode shape recognition using image processing, Journal of Sound and Vibration 326 (2009) 909–938.

[24] T. Siebert, R. Wood, K. Splitthof, High speed image correlation for vibration analysis, Journal of Physics: Conference Series 181 (2009), 1-8.

[25] T. Siebert, M.J. Crompton, Application of high speed digital image correlation for vibration mode shape analysis, Proceedings of the SEM Annual Conference June (2010) Indianapolis, Indiana USA.

[26] W. Wanga, J. E. Mottershead, A. Ihle, T. Siebert, H. Reinhard Schubach, Finite element model updating from full-field vibration measurement using digital image correlation, Journal of Sound and Vibration 330 (2011) 1599–1620.

[27] M.N. Helfrick, C. Niezrecki, P. Avitabile, T. Schmidt, 3D digital image correlation methods for full-field vibration measurement, Mechanical Systems and Signal Processing 25 (2011) 917–927.

[28] W. Wang, J.E. Mottershead, T. Siebert, A. Pipino, Frequency response functions of shape features from full-field vibration measurements using digital image correlation, Mechanical Systems and Signal Processing 28 (2012) 333–347.

[29] P. Lava, S.Cooreman, S.Coppieters, M.DeStrycker, D.Debruyne, Assessment of measuring errors in DIC using deformation fields generated by plastic FEA, Optics and Lasers in Engineering 47 (2009) 747–753.

[30] P. Lava a, S.Cooreman, D.Debruyne, Study of systematic errors in strain fields obtained via DIC using heterogeneous deformation generated by plastic FEA, Optics and Lasers in Engineering 48 (2010) 457–468.

[31] P. Lava a, S.Coppieters, Y.Wang, P.VanHoutte , D. Debruyne, Error estimation in measuring strain fields with DIC on planar sheet metal specimens with a non-perpendicular camera alignment, Optics and Lasers in Engineering 49 (2011) 57–65.

[32] Y. Wang, P. Lava, S. Coppieters, M. De Strycker, P. Van Houtte, D. Debruyne, Investigation of the uncertainty of DIC under heterogeneous strain states with numerical tests, Strain (2012), 1-10.

[33] E.A. Patterson, E. Hack, P. Brailly, R.L. Burguete, Q. Saleem, T. Siebert, R.A. Tomlinson, M.P. Whelan, Calibration and evaluation of optical systems for full-field strain measurement, J Optics and Lasers in Engineering, 45(5) (2007) 550-564.

[34] A. Davighi, R. Burguete, M. Feligiotti, E. Hack, S. James, E. Patterson, T. Siebert, M. Whelan, The development of a reference material for calibration of full-field optical measurement systems for dynamic deformation measurements, Applied Mechanics and Materials 70 (2011) 33-38.

[35] E. Hack, G. Lampeas, J. Mottershead, □. P□tterson, T. Siebert, M. Whelan, Progress in developing a standard for dynamic strain analysis, Experimental and Applied Mechanics, Conference Proceedings of the Society for Expe□imental□Mec□ani□s Series 9999 (6) (2011)□425-429.

[36] P.L.Reu, Experimental and numerical methods for exact sub p□xel□shi□tin□, J Experimental Mechanics, 51 (2011) 443–45IJ.

[37□ H.W. Schreier, M□A. Sutton, Systematic errors in digital image correlation due to under matched subset shape functions, J Experimental Mechanics 42(3) September (2002) 303- 310.

[38] B. Pan, K. Qian, H. Xie, A. Asundi, Two-dimensional digital image correlation for in-plane displacement and strain measurement: a review, Meas. Sci. Technol. 20 (2009) 062001.

[39] W.L. Briggs, V. Emden Henson, The DFT: An Owners' Manual for the Discrete Fourier Transform, chapter3, 1995.

[40] M. A. Sutton, J. J. Orteu, H. W. Schreier, Image correlation for shape, motion and deformation measurements–Basic concepts, theory and applications, Springer 2009.

[41] R.G. Lyons, Understanding Digital Signal Processing, Addison Wesley, 1997.

[42] P. Anbalagan, M. Sundarambal, A.V. Hari Prasad, Development of Interpolation Algorithms for Multirate Signal/Image Processing, Intergrated Systems with Multiploe Techniques, 161 (1998).

[43] P. Mazzoleni, F. Matta, E. Zappa, M.A. Sutton, A. Cigada, Image filter pre-processing for uncertainty minimization in two-dimensional digital image correlation, Experimental Mechanics, (Under Review).